Global cellular response to chemical perturbation of PLK4 activity and abnormal centrosome number

Johnny M Tkach[1], Jonathan Strecker[1,2,3], Daniel Durocher[1,2] and Laurence Pelletier[1,2*]

[1]Lunenfeld-Tanenbaum Research Institute, Sinai Health System, 600 University Avenue, Toronto, ON M5G 1X5, Canada
[2]Department of Molecular Genetics, University of Toronto, Toronto, ON M5S 1A8, Canada
[3]Current address: Broad Institute of MIT and Harvard, Cambridge, MA 02142, USA

[*]Corresponding author: pelletier@lunenfeld.ca

Running title: Response to altered PLK4 activity and centrosome number

Key words: Centrosome, centriole, PLK4, TRIM37, E3 ligase

Word count: 5315

ABSTRACT

Centrosomes consist of two centrioles surrounded by pericentriolar material and are the main microtubule organizing centre in metazoans. Centrosome number is tightly regulated by limiting centriole duplication to a single round per cell cycle. This control is achieved by multiple mechanisms, including the regulation of the protein kinase PLK4, a master regulator of centrosome biogenesis. In an evolutionarily conserved process, altered centrosome numbers cause a p53-dependent growth arrest through mechanisms that are still poorly defined. To gain insights into this process, we used a series of genome-wide CRISPR/Cas9 screens to identify factors important for growth arrest after chemically altering PLK4 activity to cause too many or too few centrosomes. We identify TRIM37 as a key mediator of growth arrest when PLK4 activity is partially or fully inhibited but is not required for growth arrest triggered by supernumerary centrosomes. Moreover, this activity is independent of its role as an E3 ligase and distinct from other TRIM37 functions described to date. We propose that altered PLK4 activity itself can signal growth arrest.

INTRODUCTION

The centrosome is a multi-protein complex that is the major microtubule nucleating centre (MTOC) of metazoan cells influencing microtubule-based processes such as cell division, ciliogenesis, signaling and cell motility [1]. Each centrosome consists of two microtubule-based centrioles surrounded by pericentriolar material (PCM) [1]. Each cell inherits a single centrosome from the previous cell cycle and subsequent centriole duplication is restricted to a single round of replication [2]. Centriole duplication initiates at the G1/S transition, concomitant with the timing of DNA replication and is largely a step-wise pathway dependent on the master regulating kinase PLK4 [2]. PLK4 is a low-abundance protein[3] that is recruited around the mother centriole through interactions with CEP152 and CEP192 [4, 5]. PLK4 kinase activity is regulated by interaction with STIL and CEP85 resulting in the recruitment of SASS6 to form the cartwheel of the nascent daughter centriole [6-8]. CENPJ[9-11], CEP120, SPICE[12] and POC5[13] are subsequently recruited to mediate centriole elongation. PLK4 functions as a homodimer and autophosphorylates itself in trans on Ser305 to generate a phospho-degron sequence that limits its abundance. This sequence is recognized by $SCF^{\beta\text{-TrCP}}$ and targets PLK4 for ubiquitin-mediated proteolysis [14-16].

PLK4 misregulation is often associated with pathological states. Centrosome amplification is a hallmark of tumour cells [17] and may play a role in generating chromosome instability [18, 19] and cell invasiveness [20]. In cell culture and mouse models, overexpression, inhibition or deletion of PLK4 results in p53-dependent arrest [21-29]. A series of CRISPR/Cas9 screens identified mediators of arrest after centriole loss including p53 pathway members, p53, p21(CDKN1A), 53BP1 and USP28. [22, 24, 30], with two groups also identifying TRIM37 [24, 30]. A recent screen for mediators of supernumerary centrosome-induced arrest identified PIDDosome/p53 and placed the distal appendage protein ANKRD26 within this pathway [31].

TRIM37 is an E3 ligase that is associated with gene expression [32], peroxisome maturation [33], various signaling pathways [34-36] and centriole duplication [37]. A number of centrosome-centric TRIM37 functions have been recently described. In the absence of TRIM37 a collection of centriole proteins such as CNTROB, PLK4, CETN1/2, CP110 accumulate to form aberrant assemblies referred to as condensates or 'Cenpas' (Centriolar protein assemblies) [38, 39]. These structures are dependent on the presence of CNTROB, but it is unclear why TRIM37 might suppress their formation in normal cells TRIM37 is part of the 17q23 amplicon present in approximately 18% of breast cancer tumours [40] and overexpression of TRIM37 in these lines renders them sensitive to the PLK4 inhibitor centrinone [41, 42]. TRIM37 was found to form complexes with both PLK4 and CEP192 [41]. Although TRIM37 also mediates the ubiquitination of PLK4, this modification did not result in changes to PLK4 abundance[41]. In contrast, TRIM37 association with CEP192 leads to its ubiquitination and subsequent degradation[41, 42]. In this model of TRIM37 function, PLK4-nucleated condensates consisting of PCM components facilitate mitosis in the absence of TRIM37 and the overexpression of TRIM37 decreases the cellular levels of CEP192 rendering cells sensitive to the loss of centrioles.

We sought to determine how growth arrest is initiated in response to alterations in PLK4 activity and centrosome number. Using the specific PLK4 inhibitor, centrinone B we modulated PLK4

activity to generate supernumerary centrosomes or to induce centriole loss and performed genome-wide chemical genetic screens in RPE-1 and A375 cells. Our screens identified distinct pathways mediating the response to partial and full PLK4 inhibition. Intriguingly, TRIM37 was required for growth in the absence of centrosomes and in the presence of partially inhibited PLK4, but was dispensable for arrest triggered by supernumerary centrosomes. We propose that an E3 ligase-independent activity of TRIM37 underlies its growth arrest function.

RESULTS

Centrinone induces concentration-dependent changes in centrosome number

Centrinone is a PLK4-specific inhibitor that has been used to study the cellular response to centrosome loss[23]. Another PLK4 inhibitor, CFI-400945, induces both centrosome amplification or loss in a concentration-dependent manner [43]. Since CFI-400945 also inhibits other mitotic kinases such as AURKB [44] it was unclear if this was due to effects on PLK4, mitosis, or both. To address this, we used centrinone B since its specificity towards PLK4 over AURKA and B is 2- and 5-fold greater than centrinone, respectively [23, 44]. We treated RPE-1 hTERT cells, a near diploid retinal pigment epithelial cell line, with centrinone B and monitored cell growth (Figure 1A). Cell growth was inhibited at concentrations above 150 nM with full inhibition observed at concentrations greater than 200 nM. As expected, cell growth arrest was correlated with induction of p53 and p21 (Figure 1B, Figure 1 -figure supplement 1A), resulting in the accumulation of cells in with 1 N DNA content (Figure 1 – figure supplement 1B). We next imaged cells treated with centrinone B for 3 days to determine how centrosome number was affected as a function of centrinone B concentration. As expected, high doses of centrinone B resulted in centrosome loss, but cells treated with low doses failed to lose centrosomes and in fact, accumulated supernumerary centrosomes in approximately 50% of cells (Figure 1 C, D and E). Staining for a panel of centriole and centrosome markers revealed that these extra structures contained CEP135, CEP120, CETN2, glutamylated tubulin and could accumulate PCNT and CEP192 indicating that moderate centrinone B induces *bona fide* centrosomes (Figure 1 – figure supplement 1C). Together, these data indicate that while centrosome number can be modulated positively or negatively using low or high doses of centrinone B, respectively, both conditions result in p53-dependent G1 arrest.

Global cellular responses to abnormal centrosome number

To understand the mechanisms that facilitate centrinone-induced cell cycle arrest we performed genome-wide CRISPR screens using the TKOv1 library (Figure 2A) [45]. We reasoned that loss of genes upstream of the p53 pathway would result in increased survival in the presence of drug. Since loss of components in the p53 pathway itself would also increase fitness in the presence of centrinone, we performed a parallel screen in the presence of Nutlin-3a, a small molecule that prevents the MDM2-mediated inactivation of p53 and thus artificially activates the p53 pathway [46]. Therefore, hits from the centrinone screen that also occur in the Nutlin-3a screen are likely members of p53-specfic pathways. RPE-1 cells stably expressing Cas9 were infected with the virus library, selected and subsequently treated with the indicated drug for 21 days (Figure 2A). After growth, cells were harvested and subjected to next-generation sequencing (NGS) and Model-based Analysis of Genome-wide CRISPR-Cas9 Knockout (MAGeCK) analysis [47]. Genes with a false discovery rate (FDR) of < 0.05 were considered hits for subsequent analyses. The screens to identify regulators of growth arrest using low and high centrinone B and Nutlin-3a yielded 61, 11 and 57 high-confidence hits that positively or negatively affected cell growth (Table S1), respectively.

The groups of genes identified by each screen were overlapping but distinct indicating that cells respond differently to each condition tested (Figure 2B, Figure 2 – figure supplement 2A). To

globally interrogate our dataset, we initially grouped genes by their effect as suppressors or synthetic interactors in each condition and performed Gene Ontology (GO) term and pathway enrichment analyses (Figure 2 – figure supplement 1A-D, Table S2). We observed that TP53, TP53BP1, USP28, and CDKN1A, were required for the high centrinone concentration dependent growth arrest, as has previously been described [22, 30], and were also required for growth arrest after low doses of centrinone B. Critically, the same genes were suppressors in our Nutlin-3a screen suggesting that they act in a general p53 pathway. We also found that genes involved in the centrosome cycle and those involved in regulating microtubules were required for low dose centrinone B growth arrest. However, deletion of the TSC complex (TSC1/TSC2), which has previously been implicated in p53 signaling [48, 49], sensitized cells to Nutlin-3a. Together, our datasets revealed the biological pathways involved in centrosome homeostasis control and the pathways required when these controls are compromised.

We further characterized this dataset by identifying key genes, pathway members or complexes identified in each condition. As previously observed, disruption of TRIM37 promoted growth in the absence of centrosomes [24, 30]. Additionally, TRIM37 was the only gene to score in both centrinone B conditions, but not in the presence of Nutlin-3a (Figure 2B, Figure 2 – figure supplement 2A). We noted that our CRISPR screening method was rigorous enough to identify multiple components of complexes and pathways. Core genes involved in centriole duplication (STIL, CEP85 and CENPJ) [2] and those known to affect centriole number (USP9X, PIBF1 and KIAA0753) [50-52] were identified as suppressors of arrest in the presence of extra centrosomes (Table S1, Figure 2B). In addition, we identified the entire PIDDosme (CASP2, PIDD1, CRADD) plus the newly identified member of this pathway, ANKRD26, as suppressors in these conditions [53] [31, 54]. Additionally, the disruption of AHR, ARNT and AIP that form a complex to regulate gene expression also promoted growth in the presence of extra centrosomes (Figure 2 – figure supplement 1E).

Three other screens have been performed that assessed suppressors of growth arrest due to centrosome loss and identified 31, 41 and 27 genes [22, 24, 30]. Of the seven suppressors identified here under the same conditions, four (TP53, TP53BP1, USP28, CDKN1A) correspond directly to the p53 pathway (Figure 2 – figure supplement 2F). Two of these screens also identified TRIM37 with Fong *et al* also implicating CHD8 and FBXO42 in the response to centrosome loss. While scoring in centrinone B screens, CHD8 and FBXO42 also scored in our Nutlin-3a screen suggesting that these genes might regulate the p53 pathway and may not be specific to centrosome biology. Indeed, both FBXO42 and CHD8 negatively regulate p53 activity [55, 56]. A screen for suppressors of supernumerary centrosomes has also been performed using doxycycline-inducible PLK4 [31] where 30 high-confidence hits were identified (Table S1). Of these, ten overlap with hits from our low centrinone B screen.

We next explored core and cell-specific responses to centrinone B. To do so, we repeated the screens in A375 cells, a malignant hypotriploid skin epithelial line harbouring the BRAF V600E mutation. These screens yielded 75, 45 and 34 high-confidence hits corresponding to 200 nM centrinone B, 500 nM centrinone B and Nutlin-3a, respectively (Figure 2B, Table S1). Combined with the RPE-1 data, we identified a core of 23 genes that suppressed the growth arrest in low centrinone B (Table S1, Figure 2 – figure supplement 2B-E). This set included the p53 pathway, centriole duplication factors, centriolar satellite proteins and TRIM37. Interestingly, the A375

screen identified the additional centriole components CP110, CEP97, CEP135, CEP76 and PLK4. Conversely, the AHR/ARNT/AIP complex was identified only in RPE-1 cells. Twenty of the A375 hits also overlapped with the high-confidence hits from the recent PLK4-overexpression screen (Figure 2 – figure supplement 2G) [31]. A core set of five genes (TP53, TP53BP1, USP28, CDKN1A and TRIM37) were required for growth arrest in the absence of centrosomes in both cell lines. While the RPE-1 screen only yielded 2 additional hits (CCDC101 and FBXO42), the A375 screen identified 30 additional proteins, although these were not enriched for specific functions. Together, our screens in different cell types allowed us to identify core sets of proteins involved in growth arrest after low or high centrinone B treatment and also highlights potential cell type specific responses.

Disruption of genes that supress growth arrest in the presence of centrinone could be acting upstream or downstream of p53 activation. To allow us to focus on pathways upstream of p53, we performed a screen using Nutlin-3a to identify potential regulators downstream of p53. This data set itself likely contains novel regulators of p53 signalling. The deletion of both BAG6 and EP300 resulted in increased survival when cells were challenged with Nutlin-3a. EP300 is an acetyltransferase that binds to and affects the acetylation of p53 while BAG6 modulates this acetylation by EP300 [57, 58]. As mentioned above (Figure 2 – figure supplement 1E), the AHR/ARNT/AIP complex was identified in our supernumerary centrosome screen. Inactivation of both AHT and ARNT also promoted growth when p53 is inactivated. ARNT was previously identified as a FRET interactor with p53 [59] and also interacts with EP300 [60, 61]. We used Genemania to further probe the pairwise physical interactions among the hits from the Nutlin-3a screen and generated a significantly enriched network (~20-fold enrichment, $p = 4.1x10^{-31}$). In this network, 27 of the 57 hits formed physical interactions with eight proteins forming complexes with p53 itself (Figure 2 – figure supplement 1F). Thus, our high confidence hits from the Nutlin-3a screen represent known regulators and interactors of p53 and we hypothesize that other hits could be unknown regulators of this pathway.

TRIM37 localizes near centrosomes but is not a critical centriole duplication protein

Our combined screens indicated that TRIM37 was required for growth arrest in response to a gradient of PLK4 inhibition that results in either centrosome over-duplication or loss. Since TRIM37 has been implicated in centriole duplication [37], we determined if loss of TRIM37 affected centrosome number after treatment with centrinone B. RPE-1 cells were infected with viruses expressing two independent sgRNAs targeting TRIM37 and selected cell pools were treated with 200 and 500 nM centrinone B and assessed for centriole number (Figure 3A). As previously observed [37], we noted a small number of *TRIM37*-disrupted cells harboured extra centrioles. However, centriole amplification or loss after centrinone B treatment was unaffected. To further characterize TRIM37, we created a *TRIM37*-disrutped RPE-1 cell line using CRISPR/Cas9 (Figure 3 – figure supplement 1A and B). After treatment of cells with centrinone B, p53 and p21 failed to accumulate in *TRIM37*$^{-/-}$ cells at either dose (Figure 3B). Notably, a small amount of MDM2 is cleaved in untreated *TRIM37*$^{-/-}$ cells with no additional increase after 200 nM centrinone B. This cleavage product is lost after treatment with a higher dose of centrinone. Thus, we find that TRIM37 does not affect gain or loss of centrosomes after centrinone B treatment, but is required for the induction of both p53 and p21 in response to these treatments as previously observed [30].

Since TRIM37 was a prey for multiple baits in our previous BioID survey of centrosomal proteins [62], we determined if TRIM37 localized to centrosomes. Immunofluorescence staining against endogenous TRIM37 indicated that the protein was associated with the centrosome in a subset of interphase and mitotic cells (Figure 3C). More specifically, TRIM37 localized at or near the PCM as judged by co-staining with γ-tubulin. Since centrosomal TRIM37 was not observed in all cells, we performed co-staining with either CETN2 or CEP120 to distinguish cell cycle stage (Figure 3D). We detected TRIM37 in cells harbouring two CETN2 foci or one CEP120 focus (representing G1) and in cells with three or four CETN2 foci or two CEP120 foci (representing S/G2) suggesting that TRIM37 centrosomal localization is not strictly cell cycle dependent. Additionally, TRIM37 did not preferentially decorate either mother or daughter centriole, but was often found between CETN2 foci of a single centriole. Interestingly, in cells with two centrosomes, TRIM37 appeared to favour one centrosome over the other. Given that the fluorescence signal from detecting endogenous protein was low we performed 3D-SIM on RPE-1 Cas9 *TRIM37*$^{-/-}$ cells stably expressing FLAG-BirA-TRIM37 (FB-TRIM37) (Figure 3E). FB-TRIM37 formed partial ring structures preferentially surrounding one of the γ-tubulin foci. Moreover, the FB-TRIM37 signal was discontinuous with a dot-like distribution around the ring. Thus, TRIM37 localizes to an area near the centrosomes proper, surrounding the PCM.

An E3-independent TRIM37 activity mediates growth arrest after centrinone B treatment

As a member of the TRIM family of E3 ligases, TRIM37 contains an N-terminal RING domain followed by a B-box and a coiled-coil region CCR [63]. C-terminal to these domains is a MATH/TRAF domain, unique to TRIM37, and two additional predicted CCR regions (Figure 4A). Since TRIM37 was recently shown to form a complex with PLK4 [41] we performed co-immunoprecipitation experiments in RPE-1 cells using a series of FB-TRIM37 N- and C-terminal deletion mutants (Figure 4B, Figure 4 – figure supplement 1A). We found that the primary PLK4-interacting region resided C-terminal to the TRIM domains in amino acid residues 410-964 and further mapped this region to residues 505-709. Correspondingly, a TRIM37 mutant lacking this region (FB-TRIM37 Δ505-709) did not robustly interact with PLK4.

The activity of FB-TRIM37 mutants stably expressed in RPE-1 *TRIM37*$^{-/-}$ cells (Figure 4 – figure supplement 1B) was analyzed using clonogenic survival assays in the presence of centrinone B (Figure 4C, Figure 4 – figure supplement 1C). Expression of FB-TRIM37 fully restored the growth arrest triggered by centrinone B. The expression of either the TRIM domains alone (1-409) or a protein deleted for these regions (410-964) marginally suppressed the growth arrest defect. Notably, the expression of a RING domain mutant (C18R) that abolishes TRIM37-mediated ubiquitination activity [32] fully restored growth arrest. Correspondingly, a protein lacking the entire RING domain was also functional in mediating centrinone-induced growth arrest. The region sufficient for binding PLK4 (505-709) did not support growth arrest activity while the mutant lacking the PLK4-interacting region was functional. These data indicate that TRIM37 promotes growth arrest in response to centrinone B in an E3-independent manner. Moreover, this activity does not require robust complex formation with PLK4.

To validate our finding that the TRIM37 growth arrest activity was E3-independent we created TRIM37 knockout pools in RPE-1 and A375 cells using a distinct sgRNA (Figure 3 – figure supplement 1A). These pools were infected with virus to express the indicated TRIM37 mutants (Figure 4 – figure supplement 1D-F). We performed a centrinone B titration to more fully characterize the growth arrest activity promoted by TRIM37 (Figure 4D, Figure 4 – figure supplement 1G). Strikingly, at approximately 125 nM centrinone B growth arrest was observed in both WT and *TRIM37*$^{-/-}$ lines of each cell type. Cells lacking *TRIM37* suppressed the growth arrest from 150 to 500 nM centrinone B in RPE-1 and 167 to 500 nM in A375 cells. As observed with cell lines derived from the clonal TRIM37 disruption, both E3-defective mutants, C18R and ΔRING, promoted growth arrest activity as did Δ505-709. We also monitored the extent of centriole over-duplication and loss under these conditions (Figure 4 – figure supplement 1H). Surprisingly, the extent of centriole overduplication did not correlate to robust growth arrest in WT cells, or the ability of TRIM37 to mediate this arrest. The behaviour of *TRIM37*$^{-/-}$ lines at different concentrations of centrinone B prompted us to test if TRIM37 responded to excess centrioles induced by PLK4 overexpression. We created a tetracycline-inducible PLK4 system in WT, *TP53*$^{-/-}$ and *TRIM37*$^{-/-}$ RPE-1 cells and performed clonogenic survival assays (Figure 4E). Consistent with recent observations [31], loss of TRIM37 does not suppress growth arrest induced by PLK4 overexpression. Our data suggests that the growth arrest activity triggered by 150 to 500 nM centrinone B is independent of TRIM37 E3 activity and that excess centrioles might not be the trigger for this arrest at low centrinone B concentrations.

TRIM37 E3-dependent and -independent activities

These results prompted us to investigate which TRIM37 activities were dependent on its E3 ligase activity and if these functions correlated with its growth arrest activity. First, we performed live-cell imaging to measure mitotic length of cells grown in centrinone. Cells were treated with the indicated concentration of centrinone B for 3 days before imaging for 24 h and mitotic length from nuclear envelope breakdown (NEBD) to telophase was determined (Figure 5A and B). Wild type RPE-1 cells did not exhibit a significant increase in mitotic length compared to untreated until 150 nM centrinone B. Strikingly, the mitotic length of *TRIM37*$^{-/-}$ cells was similar to that of WT until 200 and 500 nM centrinone B where the absence of TRIM37 suppressed the increase in mitotic length in WT cells as previously observed [41]. We next examined whether TRIM37 E3 activity was required to rescue the shortened mitotic length observed in *TRIM37*$^{-/-}$ cells (Figure 5C and D). Expression of both FB-TRIM37 and the C18R mutant rescued the altered mitotic length after 500 nM centrinone B treatment, in contrast to previous reports [41]. The mitotic lengths of cells expressing FB-TRIM37 C18R increased at even lower centrinone B concentrations than observed with WT cells or cells expressing FB-TRIM37. We conclude that TRIM37 influence on the length of mitosis after PLK4 inhibition is neither correlated with its ability to promote growth arrest nor dependent on its E3 activity.

In the absence of TRIM37, some centriolar proteins form intracellular aggregates in interphase cells [38, 41]. We observed that CEP120, CETN2 and CNTROB, but not PLK4 could be detected in these aggregates (Figure 5 – figure supplement 1A). PLK4 has been observed in similar structures but could only be detected using a single antibody [30, 38, 39]. To verify our results, we expressed FLAG-tagged PLK4 from a tetracycline-inducible promoter in *TRIM37*$^{-/-}$ cells. We could not detect PLK4-FLAG at non-centrosomal aggregates after 3 or 6 h induction

using either anti-FLAG or anti-PLK4 antibodies, despite its accumulation at the centrosome (Figure 5 – figure supplement 1B). In mitotic cells, these structures occasionally co-localized with CEP192 (Figure 5 – figure supplement 1C). In many cells prior to anaphase the structures could nucleate or bind microtubules, but this ability was typically lost by anaphase with a concomitant loss of CEP192 at the structures. In all cells observed post-anaphase, the structures were asymmetrically inherited. Additionally, these assemblies were not acutely affected by loss of PLK4 activity as they were observed in *TRIM37*$^{-/-}$ cells treated with 500 nM centrinone B for 4 days (Figure 5 – figure supplement 1D). After re-expression of TRIM37 mutants we observed that these structures disappeared in an E3-dependent manner (Figure 5E, Figure 5 – figure supplement 1E and F). Importantly, the structures visible in interphase appear to be distinct from those observed in mitotic *TRIM37*$^{-/-}$ cells after PLK4 inhibition [30]. Here, amorphous collections of primarily PCM components act as pseudo-MTOCs. We treated cells stably expressing TRIM37 mutants with 500 nM centrinone B before imaging PCNT and CEP192. Cells lines that contained functional TRIM37 as judged by clonogenic assays also accumulated a higher percentage of mitotic cells in prophase (Figure 5F). Consistent with this observation, cell lines with non-functional TRIM37 formed ectopic MTOCs that arranged in a pseudo-bipolar manner (Figure 5G, Figure 5 – figure supplement 2A). Cell lines expressing functional TRIM37 primarily formed either a monopolar structure around a single existing centriole or displayed an acentriolar mitosis absent of ectopic PCM formations (Figure 5G, Figure 5 – figure supplement 2B). We find that the CNTROB/CEP120 structures are dependent on TRIM37 E3 activity, but the appearance of ectopic MTOCs is correlated to growth arrest activity, not E3 activity.

It was recently suggested that TRIM37 is a negative regulator of CEP192 abundance [41, 42]. We probed for PCM components in RPE-1 and RPE-1 *TRIM37*$^{-/-}$ lines (Figure 6A) and RPE-1 *TRIM37*$^{-/-}$ lines stably over-expressing WT FB-TRIM37 or FB-TRIM37 RING mutants (Figure 6B) but did not detect any changes in the total abundance of the major PCM components CEP192, PCNT or CDK5RAP2. In previous reports acute over-expression of TRIM37 was used to detect changes in PCM proteins. To reproduce these conditions, we expressed WT or C18R TRIM37-3xFLAG in WT RPE-1 cells using a doxycycline-inducible system. After expression of WT TRIM37 for 4 or 8 h we detected a 50 to 75% decrease in total CEP192 protein (Figure 6C, left panels). Similar results were obtained after induction for 48 and 72 h (right panels), although the decrease in total CEP192 was more modest. In all cases the decrease in CEP192 was E3 dependent. We also analyzed these cells using immunofluorescence to specifically detect changes at mitotic centrosomes. Quantification revealed that over expression of WT TRIM37, but not C18R decreased the intensity and area of CEP192 (Figure 6D, Figure 6 – figure supplement 1B) and PCNT (Figure 6 – figure supplement 1A and B) at the centrosome. Interestingly the centriole component CEP120 was also similarly affected indicating that this effect is not specific to PCM proteins (Figure 6D and Figure 6 – figure supplement 6B). We find that acute over-expression of TRIM37 affects the overall abundance of CEP192 and the mitotic accumulation of some centrosome and centriolar proteins in an E3-dependent manner.

Our results confirmed that PLK4 and TRIM37 form a complex in RPE-1 cells (Figure 3G). The co-expression of Myc-PLK4 and T7-TRIM37 in HEK293T cells resulted in an E3-dependent modification of PLK4 that was not readily detected in RPE-1 cells (Figure 7A). The modification was mostly dependent on TRIM37 E3 activity, was not observed when TRIM37 505-709 was expressed, and increased in the presence of TRIM37 Δ505-709. Treatment with the general SCF

inhibitor MLN4924 [64] resulted in general stabilization of these forms (Figure 7A). PLK4 is known to harbour both ubiquitination and phosphorylation modifications where phosphorylation precedes its ubiquitination [14-16, 65]. To identify the modification type, we first co-expressed Myc-PLK4, T7-TRIM37 and HA-Ub. After immunoprecipitating PLK4 we probed for HA-Ub to detect ubiquitinated species (Figure 7B). Although we detected an E3-dependent increase in total ubiquitination in the input of cells expressing WT and Δ505-709 T7-TRIM37, we only detected a minor amount of HA-Ub in the immunoprecipitates. To determine if PLK4 was phosphorylated, we treated lysates with λ-phosphatase (Figure 7C). The modified PLK4 was entirely lost after phosphatase treatment indicating that this form is primarily due to phosphorylation. To identify the kinase responsible for the modification we treated cells with inhibitors targeting PLK4, AURKA, PLK1 and CDK1 for 3 to 6 h and probed for PLK4 (Figure 7D). Although treatment with the CDK1 inhibitor RO-3066 had a minor effect on PLK4 phosphorylation, this modification was almost entirely abolished after PLK4 inhibition. Our data suggest that TRIM37 and PLK4 can form a complex and that TRIM37 promotes the stabilization of phosphorylated PLK4 in an E3-dependent manner.

DISCUSSION

Cells harbouring abnormal centrosome numbers are usually subject to p53-dependent growth arrest. Although these arrest pathways are beginning to be uncovered, the global response to centriole abnormalities remains unknown. Here, we used centrinone B, the most specific PLK4 inhibitor available, to modulate PLK4 activity and performed chemical-genetic screens to identify genes required for the subsequent growth arrest. TRIM37 was required for the growth arrest in response to partially and fully inhibited PLK4, but this activity was independent of the presence of excess centrioles. We suggest that an E3-independent TRIM37 activity is at least partly required for its growth arrest function.

Current models of TRIM37 function posit that increased mitotic length in the absence of centrioles eventually leads to growth arrest and that the absence of TRIM37 suppresses this increase [41, 66]. We identified three distinct pathways leading to growth arrest after PLK4 inhibition. First, at 125 nM centrinone B we did not observe a significant increase in RPE-1 mitotic length despite cells arresting in G1 under these conditions; however, this arrest is also independent of TRIM37 and centriole number abnormalities and will be the subject of further investigation. As cells were treated with higher doses of centrinone B, we observe a TRIM37-dependent growth arrest without a corresponding difference in mitotic length between WT and *TRIM37*$^{-/-}$ cells followed by a second TRIM37-dependent growth arrest where loss of TRIM37 suppresses an increased mitotic length. These observations leave open the possibilities that either mitotic length is unimportant for growth arrest, or that there are different signals for arrest and/or arrest bypass after partial PLK4 inhibition compared to full inhibition. We note, however, any increases in mitotic length were relatively minor and typically shorter than 90 minutes, a length that should not activate a 'mitotic timer' in this cell type [67].

Proteins can be poly- or monoubiquitinated resulting in changes to protein abundance or activity [68]. The role of TRIM37 E3 activity to its overall function is unclear since it has been reported to mediate both poly- and monoubiquitination resulting stabilization [33] and destabilization [39, 41, 42, 69] of targets as well as altering target function [32, 70, 71]. Additionally, an E3-

independent role in autophagy has also been described [72]. We found that TRIM37 E3 activity was required for its role in interphase condensate/Cenpas dissolution and for its role in CEP192 stability as previously observed. Since TRIM37 E3 activity is dispensable for proliferation arrest caused by centrinone B, we conclude that these activities do not play a vital role in this process on their own. Interestingly, the suppression of ectopic, mitotic MTOCs in acentriolar *TRIM37*$^{-/-}$ cells was not dependent on TRIM37 E3 activity and correlated well with growth arrest activity. The differential dependence of condensates/Cenpas and ectopic MTOC on TRIM37 E3 activity suggests that these structures behave independently. It remains unclear how ectopic MTOCs might promote growth after PLK4 inhibition. Since these structures are only observed after centriole loss, it is possible they specifically suppress the increased mitotic length in acentriolar cells with different mechanisms operating at lower centrinone B concentrations. Alternatively, these structures may be indicative of another process that is altered in TRIM37$^{-/-}$ cells. TRIM37 role in autophagy is the only other E3-independent function described [72]. Since supernumerary centrosomes disrupt autophagy [73] it is tempting to speculate that increased autophagy flux in *TRIM37*$^{-/-}$ cells underlie its role in suppressing growth arrest after PLK4 inhibition.

Partial inhibition of PLK4 by CFI-400495 [43], YLT-11[74] or centrinone paradoxically results in centrosome amplification. The model proposed to explain this observation suggests that partial inhibition reduces PLK4 autophosphorylation and therefore also reduces its degradation [75]. In this scenario, the increased abundance of PLK4 results in a greater overall activity despite the inhibition and therefore has outcomes similar to PLK4 overexpression and will result in p53-dependent growth arrest. Our results with TRIM37 show that this explanation is likely oversimplified. Between 150 to 200 nM centrinone B, we observe an increase in centrosome number and a corresponding dependence on TRIM37 for growth arrest, yet TRIM37 is dispensable for growth arrest after PLK4 overexpression; thus there is a disconnect between centriole amplification, growth arrest and TRIM37 status. The combination of our data and a recent screen for mediators of growth arrest after PLK4 overexpression [31] yields a minimal set of 10 genes required for growth arrest in the presence of supernumerary centrosomes that include the ANKRD26/PIDDosome complex. We suggest that the remaining genes unique to our dataset, including TRIM37, might be required for a response to altered PLK4 activity itself. CEP85 and USP9X are among these genes and both affect STIL, a regulator of PLK4 activity. CEP85 is required for robust STIL interaction with PLK4 while USP9X stabilizes STIL. [8, 76]. Our data show that overexpression of TRIM37 stabilizes PLK4 phosphorylation and is therefore also poised to affect or detect PLK4 activity. Since robust interaction between TRIM37 and PLK4 was not required for accumulation of phosphorylated PLK4 we propose that TRIM37 may block PLK4 dephosphorylation or ubiquitination. TRIM37 E3 function is proposed to underlie the increased sensitivity of breast cancer cells to PLK4 inhibition [41, 42] In these models, E3-dependent, TRIM37-mediated degradation of CEP192 underlies these sensitivities, however, it was not formally tested if overexpression of an E3 mutant version of TRIM37 results in the same hypersensitivity to centrinone. TRIM37 clearly has pleiotropic effects on centrosome biology that are both E3-dependent and -independent; further studies that tease these functions apart will be useful in resolving TRIM37 function in normal and disease states.

ACKNOWLEDGEMENTS

We thank members of the Pelletier lab for scientific feedback during the preparation of this work. We are grateful to Sally Cheung and Suzanna Prosser for proofreading the manuscript. The rabbit and rat CEP120 antibodies and CEP135 antibody were generous gifts from Li-Heui Tsai, Moe Mahjoub and Alex Bird, respectively. The TKOv1 virus library was generously provided by Jason Moffat. The pcDNA3 HA-ubiquitin plasmid was constructed by Abdallah Al-Hakim in the lab of Dan Durocher. This work was funded through a Canadian Institute for Health Research Foundation Grant, an ORF RE-5 grant from the Ontario Ministry for Research, and a grant-in-aid from the Krembil Foundation. L.P. holds a Tier 1 Canada Research Chair in Centrosome Biogenesis and Function.

AUTHOR CONTRIBUTIONS

L.P and J.M.T conceived the project and designed experiments. J.S and J.M.T. performed the CRISPR/Cas9 screens. J.M.T. performed all other experiments. L.P. and J.M.T. interpreted and analyzed the results. L.P. and J.M.T wrote the manuscript. L.P., J.M.T, J.S. and D.D. reviewed and edited the manuscript. D.D. supervised J.S.

DECLARATION OF INTERESTS

The authors declare that DD is a shareholder of Repare Therapeutics and DD and LP are consultants to Repare Therapeutics.

MATERIALS AND METHODS

Cell culture and drug treatments

All cell lines were cultured in a 5% CO2 humidified atmosphere at 37°C. HEK293T (female, human embryonic kidney epithelial) cells are from ATCC. hTERT-RPE1 (female, human epithelial cells immortalized with hTERT) and A375 cells (female, human malignant melanoma epithelial) stably expressing Cas9 were a kind gift from D. Durocher. hTERT-RPE1, HEK293T and A375 were grown in Dulbecco's Modified Eagle's Medium (DMEM; Gibco) supplemented with 10% (v/v) fetal bovine serum (FBS; Gibco) and 2 mM Glutamax (Gibco). PLK4 inhibitor centrinone B (Tocris) was used as described. Nutlin-3a (Cayman Chemical) was used at 600 nM. The CDK1, PLK1 and Aurora A kinase inhibitors RO-3306 (Enzo Life Sciences), BI-2536 (ChemieTek) and MLN8237 (Selleck Chemicals) were used at 10 μM, 100 nM and 200 nM, respectively.

Viral methods

To produce lentivirus, $4x10^6$ HEK293T were seeded in a T-75 flask and transfected with 4 μg of the appropriate transfer vector, 3 μg psPAX2 and 2μg pCMV-VSV-G using 18 uL each Lipofectamine 3000/P3000 reagent (Invitrogen). After 24 h, growth medium was replaced with fresh medium containing 30% FBS and viral supernatant was collected after a further 48 h. Virus was stored at -80°C. To generate cell lines, 200 k cells were seeded with viral supernatant and 4 μg/mL polybrene (MilliporeSigma). Medium was changed after 24 h and appropriate drug selection was added after an additional 24 h where required.

CRISPR/Cas9 screening

CRISPR screens were performed as described [45, 77]. Briefly, Cas9-expressing cells were transduced with the TKOv1 viral library (~90 k sgRNA) [45] at low MOI (~0.3) in the presence of 4 μg/mL polybrene. RPE-1 cells were selected as described [78]. A375 cells were selected using 2 μg/mL puromycin. $10x10^6$ cells were harvested four days post-transduction and represents day 0. Cells were grown for 6 days before being split for drug treatment in technical triplicate and further grown for 21 days. A library coverage of > 100 cells/sgRNA was maintained at each step. gDNA from cell pellets was isolated using a QIAamp Blood Maxi Kit (Qiagen) and genome-integrated sgRNA sequences were amplified using the KAPA HiFi HotStart ReadyMix (Kapa Biosystems). Sequencing libraries were made by addition of i5 and i7 multiplexing barcodes in a second round of PCR and the product gel purified using QIAquick Gel Purification kit (Qiagen). Libraries were sequenced using Illumina HiSeq2500 or NextSeq500. Sequence data was analyzed using MAGeCK [47] to determine sgRNA distribution among the samples. Drug-treated samples at 21 days post-drug addition were compared to DMSO-treated cells at 12 days post-drug addition to equalize the number of cell doublings. Genes with FDR < 0.05 were used for further analysis.

Network analysis and gene enrichment

High-scoring genes from MAGeCK analysis were visualized using Cytoscape [79]. General node arrangement was performed using the yFiles Organic Layout and manually modified to facilitate visualization. Each screen condition (200 nM centrinone B, 500 nM centrinone B and Nutlin-3a) was considered as a source node, corresponding hits as target nodes and FDR as edge attributes. Genes from the indicated data sets were analyzed using the ClueGo app within Cytoscape [80]. Enrichments for Biological Function (circles) or Cellular Component (hexagons) based on all experimental evidence was determined. Only pathways with p-value < 0.05 are shown. Nodes arranged using the yFiles Organic Layout.

CRISPR/Cas9 gene disruption

For lentivirus-mediated gene disruption of *TRIM37*, sgRNA sequences were cloned into plentiGuide-Puro as described [81]. RPE-1 Cas9 cells were infected with lentiviral particles and selected as described above. Clonal *TRIM37*$^{-/-}$ lines were generated using *in vitro* transcribed (IVT) sgRNA. IVT templates were created by PCR using cr_tracrRNA, IVT forward, IVT reverse and sgRNA-specific oligonucleotides (TRIM37 sgRNA 1). PCR products were used directly as templates for IVT using HiScribe T7 transcription kit (NEB). Resulting RNA was purified using RNAClean XP beads (Beckman Coulter) and used to transfect RPE-1 cells using RNAiMAX (ThermoFisher) according to manufacturer's instructions. Clonal lines were generated by limiting dilution and assessed for gene disruption by Western blot and TIDE [82] or Synthego ICE (Synthego Performance Analysis, ICE Analysis. 2019. v2.0. Synthego; accessed 9/19/2018) analyses. *TRIM37*$^{-/-}$ pools in RPE-1 and A375 cells were generated similarly using an sgRNA targeting exon 5. After transfection, cells were grown in medium containing 500 nM centrinone B for two weeks before growth in normal medium.

Immunofluorescence staining, microscopy and quantification

Cells were grown as indicated on No. 1.5 coverslips, washed once with PBS and fixed with -20°C methanol for at least 10 min. All subsequent steps performed at room temperature. Coverslips were rinsed with PBS and blocked with antibody solution (PBS, 0.5% (w/v) BSA and 0.05% Tween-20) for 15 to 30 min. Samples were incubated with primary antibodies (Table S3) for 1 h, washed 3 x 5 min and incubated with secondary antibodies (Table S3) and DAPI (0.1 μg/mL) for 45 min. Coverslips were washed 3 x 5 min and mounted on slides using Prolong Gold (Invitrogen). Deconvolution wide-field microscopy was performed using the DeltaVision Elite system equipped with an NA 1.42 60x PlanApo objective (Olympus) and an sCMOS 2048 x 2048 camera (Leica Microsystems). Each field was acquired with a z-step of 0.2 μm through the entire cell and deconvolved using softWoRx (v6.0, Leica Microsystems). Maximum intensity projections are shown (0.1080 μm/pixel). Display levels are the same for all images in a panel unless otherwise indicated.

Quantification pipelines were created using CellProfiler 3.0 [83] (www.cellprofiler.org). Each image was manually cropped to include only a single mitotic cell. Each channel was background subtracted using the lower quartile intensity of the entire image and the signal was segmented

into objects using a robust background thresholding. The area and integrated intensity of each object was measured.

For live imaging, 15 000 cells were seeded per well in an 8-well Lab-Tek II chamber slide. The next day fresh medium containing drug was added and cells incubated for 3 days. Fresh medium containing indicated drug and 200 nM SiR-DNA (Spirochrome) was added for 2 h before imaging. Microscopy was performed using the DeltaVision Elite system equipped with an NA 0.75 U Plan S-Apo objective (Olympus) and an sCMOS 2048 x 2048 camera. Each field was acquired with 6 x 2 μm z-step every 5 min for 24 h. The time between nuclear envelope breakdown and full chromosome separation judged by nuclear morphology was quantified.

Super-resolution microscopy was performed on a three-dimensional structured-illumination microscope (3D-SIM) (OMX Blaze v4, Leica Microsystems) as described[84].

Western blot

Cells were grown as indicated, washed once with PBS and resuspended directly in 2x SDS-PAGE sample buffer containing Benzonase (0.25 U/μL, MilliporeSigma) and heated at 95°C for 5 min. Proteins (typically 10 to 20 μg) were separated by SDS-PAGE and transferred to PVDF using a wet transfer apparatus (Bio-Rad). Total protein was detected by staining with PonceauS (MilliporeSigma) and scanning. All steps performed at room temperature unless indicated. Blocking and primary antibody incubations were performed using TBS-T (TBS + 0.05% Tween-20) with 0.5% skim-milk powder (Bioshop). Membranes were blocked for 30 min and incubated with primary antibody (Table S3) overnight at 4°C. After washing 3 x 5 min, membranes were incubated with secondary antibodies for 45. HRP-conjugated secondary antibodies (Bio-Rad) were incubated in TBS-T/milk for 45 min and washed 3 x 5 min with TBS-T before detecting using a Chemidoc imager (Bio-Rad). NearIR-conjugated secondary antibodies (LI-COR Biosciences) were incubated in TBS-T/milk + 0.015% SDS for 45, washed 3 x 5 min with TBS-T and 1 x 5 min with TBS before drying the membrane for 2 h at RT. Dried blots were imaged using an Odyssey CLx imager (LI-COR Biosciences).

Quantification of Western blots were performed on images obtained using NearIR secondary antibodies. Images were quantified using ImageJ [85] Gel Analysis tools and normalized to Ponceau S staining of the same lane.

Clonogenic survival assays

Two-hundred and fifty RPE-1 or 200 A375 cells were seeded in either a 10 cm dish or 6-well plate. The next day medium was removed and medium containing the indicated drug was added. After 12 to 14 days, plates were rinsed once with PBS and fixed and stained with 0.5% crystal violet (MilliporeSigma) in 20% methanol for 20 min. Plates were washed extensively with water, dried and scanned. Images were segmented using the Trainable Weka Segmentation tool [86] in ImageJ. A new model was built for each replicate if required. The resulting segmentation image was thresholded and used as a mask to overlay the original image that was inverted and

background subtracted using a 50-pixel rolling circle. The colony intensity per well or dish was then measured within the masked region.

Immunoprecipitation and protein treatments

To detect complex formation between PLK4 and TRIM37, $2x10^6$ RPE-1 cells were seeded per 10 cm dish and transfected with 3.75 µg Myc-PLK4 and 3.75 µg pcDNA5 FLAG-BirA construct using 15 µL Lipofectamine 3000/P3000 (ThermoFisher). Cells were harvested 24 h post-transfection, washed once with PBS and resuspended in lysis buffer (50 mM HEPES pH8; 100 mM KCl; 2 mM EDTA; 10% Glycerol; 0.1% NP-40; 1 mM DTT; protease inhibitors (Roche); phosphatase inhibitor cocktail 3 (MilliporeSigma)) for 30 minutes on ice. Lysates were frozen in dry ice for 5 minutes, then thawed and centrifuged for 20 minutes at 16,000xg at 4ºC. An aliquot representing the input was removed before cleared supernatants were incubated with equilibrated anti-FLAG M2 Affinity Gel (MilliporeSigma) for 1-2 hours at 4ºC. Beads were washed 3 times with lysis buffer before resuspension in 2x SDS-PAGE sample buffer. Samples were heated at 95°C for 5 min.

To probe PLK4 modification in Figures 7A, C and D, 350 000 HEK293T cells were seeded per well of a 6-well plate and transfected with 0.67 µg Myc-PLK4 and 1 µg T7-TRIM37 construct using 3.34 µL Lipofectamine 3000/P3000. Medium was changed after 24 h and cells incubated for 48 h in total before sampling. For Figure 7D, the indicated drug was added 3 and 6 h before collection. Cells were collected directly in 2x SDS-PAGE sample buffer for Figure 7A and D. For Figure 7C, cells were collected and washed once with PBS. Cells were resuspended in a modified TNTE buffer (10 mM Tris-HCl, pH = 7.4, 100 mM NaCl, 1 mM EDTA, 1 mM DTT, 0.1% TX-100; protease inhibitors; ± phosphatase inhibitor cocktail 3) and incubated for 30 min on ice before addition of $MnCl_2$ and λ-phosphatase (Bio-Rad) to the appropriate samples for 30 min at 30°C. The soluble fractions were obtained by centrifugation at 16,000 xg for 30 min. To probe for PLK4 ubiquitination, $1.5x10^6$ HEK293T cells were seeded in a 10cm dish and transfected with 2 µg Myc-PLK4, 2 µg HA-Ubiquitin and 2 µg eGFP or T7-TRIM37 with 12 µL Lipofectamine 3000/P3000. The medium was changed after 16 h and cells harvested after 48 h. Cells were washed once with PBS and resuspended in modified TNTE buffer and the soluble fraction was obtained as described above. Lysates were incubated with 3 µg anti-Myc antibodies (Table S3) and incubated for 1 h at 4°C. Equilibrated Protein G Sepharose 4 Fast Flow beads (Cytiva) were added and samples further incubated for 1 h at 4°C. Immunoprecipates were washed 3x with modified TNTE buffer and eluted by addition of 2x SDS-PAGE sample buffer and heating at 95°C for 5 min.

REFERENCES

1. Conduit, P.T., A. Wainman, and J.W. Raff, *Centrosome function and assembly in animal cells.* Nat Rev Mol Cell Biol, 2015. **16**(10): p. 611-24.
2. Gonczy, P. and G.N. Hatzopoulos, *Centriole assembly at a glance.* J Cell Sci, 2019. **132**(4).
3. Fode, C., C. Binkert, and J.W. Dennis, *Constitutive expression of murine Sak-a suppresses cell growth and induces multinucleation.* Mol Cell Biol, 1996. **16**(9): p. 4665-72.
4. Sonnen, K.F., et al., *Human Cep192 and Cep152 cooperate in Plk4 recruitment and centriole duplication.* J Cell Sci, 2013. **126**(Pt 14): p. 3223-33.
5. Kim, T.S., et al., *Hierarchical recruitment of Plk4 and regulation of centriole biogenesis by two centrosomal scaffolds, Cep192 and Cep152.* Proc Natl Acad Sci U S A, 2013. **110**(50): p. E4849-57.
6. Moyer, T.C., et al., *Binding of STIL to Plk4 activates kinase activity to promote centriole assembly.* J Cell Biol, 2015. **209**(6): p. 863-78.
7. Ohta, M., et al., *Direct interaction of Plk4 with STIL ensures formation of a single procentriole per parental centriole.* Nat Commun, 2014. **5**: p. 5267.
8. Liu, Y., et al., *Direct binding of CEP85 to STIL ensures robust PLK4 activation and efficient centriole assembly.* Nat Commun, 2018. **9**(1): p. 1731.
9. Schmidt, T.I., et al., *Control of centriole length by CPAP and CP110.* Curr Biol, 2009. **19**(12): p. 1005-11.
10. Kohlmaier, G., et al., *Overly long centrioles and defective cell division upon excess of the SAS-4-related protein CPAP.* Curr Biol, 2009. **19**(12): p. 1012-8.
11. Tang, C.J., et al., *CPAP is a cell-cycle regulated protein that controls centriole length.* Nat Cell Biol, 2009. **11**(7): p. 825-31.
12. Comartin, D., et al., *CEP120 and SPICE1 cooperate with CPAP in centriole elongation.* Curr Biol, 2013. **23**(14): p. 1360-6.
13. Azimzadeh, J., et al., *hPOC5 is a centrin-binding protein required for assembly of full-length centrioles.* J Cell Biol, 2009. **185**(1): p. 101-14.
14. Rogers, G.C., et al., *The SCF Slimb ubiquitin ligase regulates Plk4/Sak levels to block centriole reduplication.* J Cell Biol, 2009. **184**(2): p. 225-39.
15. Cunha-Ferreira, I., et al., *The SCF/Slimb ubiquitin ligase limits centrosome amplification through degradation of SAK/PLK4.* Curr Biol, 2009. **19**(1): p. 43-9.
16. Guderian, G., et al., *Plk4 trans-autophosphorylation regulates centriole number by controlling betaTrCP-mediated degradation.* J Cell Sci, 2010. **123**(Pt 13): p. 2163-9.
17. Chan, J.Y., *A clinical overview of centrosome amplification in human cancers.* Int J Biol Sci, 2011. **7**(8): p. 1122-44.
18. Ganem, N.J., S.A. Godinho, and D. Pellman, *A mechanism linking extra centrosomes to chromosomal instability.* Nature, 2009. **460**(7252): p. 278-82.
19. Silkworth, W.T., et al., *Multipolar spindle pole coalescence is a major source of kinetochore mis-attachment and chromosome mis-segregation in cancer cells.* PLoS One, 2009. **4**(8): p. e6564.
20. Arnandis, T., et al., *Oxidative Stress in Cells with Extra Centrosomes Drives Non-Cell-Autonomous Invasion.* Dev Cell, 2018. **47**(4): p. 409-424 e9.

21. Holland, A.J., et al., *The autoregulated instability of Polo-like kinase 4 limits centrosome duplication to once per cell cycle.* Genes Dev, 2012. **26**(24): p. 2684-9.
22. Lambrus, B.G., et al., *A USP28-53BP1-p53-p21 signaling axis arrests growth after centrosome loss or prolonged mitosis.* J Cell Biol, 2016. **214**(2): p. 143-53.
23. Wong, Y.L., et al., *Cell biology. Reversible centriole depletion with an inhibitor of Polo-like kinase 4.* Science, 2015. **348**(6239): p. 1155-60.
24. Fong, C.S., et al., *53BP1 and USP28 mediate p53-dependent cell cycle arrest in response to centrosome loss and prolonged mitosis.* Elife, 2016. **5**.
25. Marthiens, V., et al., *Centrosome amplification causes microcephaly.* Nat Cell Biol, 2013. **15**(7): p. 731-40.
26. Coelho, P.A., et al., *Over-expression of Plk4 induces centrosome amplification, loss of primary cilia and associated tissue hyperplasia in the mouse.* Open Biol, 2015. **5**(12): p. 150209.
27. Vitre, B., et al., *Chronic centrosome amplification without tumorigenesis.* Proc Natl Acad Sci U S A, 2015. **112**(46): p. E6321-30.
28. Sercin, O., et al., *Transient PLK4 overexpression accelerates tumorigenesis in p53-deficient epidermis.* Nat Cell Biol, 2016. **18**(1): p. 100-10.
29. Hudson, J.W., et al., *Late mitotic failure in mice lacking Sak, a polo-like kinase.* Curr Biol, 2001. **11**(6): p. 441-6.
30. Meitinger, F., et al., *53BP1 and USP28 mediate p53 activation and G1 arrest after centrosome loss or extended mitotic duration.* J Cell Biol, 2016. **214**(2): p. 155-66.
31. Evans, L.T., et al., *ANKRD26 recruits PIDD1 to centriolar distal appendages to activate the PIDDosome following centrosome amplification.* Embo j, 2021. **40**(4): p. e105106.
32. Bhatnagar, S., et al., *TRIM37 is a new histone H2A ubiquitin ligase and breast cancer oncoprotein.* Nature, 2014. **516**(7529): p. 116-20.
33. Wang, W., et al., *TRIM37, a novel E3 ligase for PEX5-mediated peroxisomal matrix protein import.* J Cell Biol, 2017. **216**(9): p. 2843-2858.
34. Zhu, H., et al., *Knockdown of TRIM37 Promotes Apoptosis and Suppresses Tumor Growth in Gastric Cancer by Inactivation of the ERK1/2 Pathway.* Onco Targets Ther, 2020. **13**: p. 5479-5491.
35. Fu, T., et al., *ASB16-AS1 up-regulated and phosphorylated TRIM37 to activate NF-kappaB pathway and promote proliferation, stemness, and cisplatin resistance of gastric cancer.* Gastric Cancer, 2021. **24**(1): p. 45-59.
36. Chen, S., et al., *TRIM37 Mediates Chemoresistance and Maintenance of Stemness in Pancreatic Cancer Cells via Ubiquitination of PTEN and Activation of the AKT-GSK-3beta-beta-Catenin Signaling Pathway.* Front Oncol, 2020. **10**: p. 554787.
37. Balestra, F.R., et al., *Discovering regulators of centriole biogenesis through siRNA-based functional genomics in human cells.* Dev Cell, 2013. **25**(6): p. 555-71.
38. Balestra, F.R., et al., *TRIM37 prevents formation of centriolar protein assemblies by regulating Centrobin.* Elife, 2021. **10**.
39. Meitinger, F., et al., *TRIM37 prevents formation of condensate-organized ectopic spindle poles to ensure mitotic fidelity.* J Cell Biol, 2021. **220**(7).
40. Kallioniemi, A., et al., *Detection and mapping of amplified DNA sequences in breast cancer by comparative genomic hybridization.* Proc Natl Acad Sci U S A, 1994. **91**(6): p. 2156-60.

41. Meitinger, F., et al., *TRIM37 controls cancer-specific vulnerability to PLK4 inhibition.* Nature, 2020. **585**(7825): p. 440-446.
42. Yeow, Z.Y., et al., *Targeting TRIM37-driven centrosome dysfunction in 17q23-amplified breast cancer.* Nature, 2020. **585**(7825): p. 447-452.
43. Mason, J.M., et al., *Functional characterization of CFI-400945, a Polo-like kinase 4 inhibitor, as a potential anticancer agent.* Cancer Cell, 2014. **26**(2): p. 163-76.
44. Suri, A., et al., *Evaluation of Protein Kinase Inhibitors with PLK4 Cross-Over Potential in a Pre-Clinical Model of Cancer.* Int J Mol Sci, 2019. **20**(9).
45. Hart, T., et al., *High-Resolution CRISPR Screens Reveal Fitness Genes and Genotype-Specific Cancer Liabilities.* Cell, 2015. **163**(6): p. 1515-26.
46. Vassilev, L.T., et al., *In vivo activation of the p53 pathway by small-molecule antagonists of MDM2.* Science, 2004. **303**(5659): p. 844-8.
47. Li, W., et al., *MAGeCK enables robust identification of essential genes from genome-scale CRISPR/Cas9 knockout screens.* Genome Biol, 2014. **15**(12): p. 554.
48. Armstrong, L.C., et al., *Heterozygous loss of TSC2 alters p53 signaling and human stem cell reprogramming.* Hum Mol Genet, 2017. **26**(23): p. 4629-4641.
49. Lee, C.H., et al., *Constitutive mTOR activation in TSC mutants sensitizes cells to energy starvation and genomic damage via p53.* Embo j, 2007. **26**(23): p. 4812-23.
50. Li, X., et al., *USP9X regulates centrosome duplication and promotes breast carcinogenesis.* Nat Commun, 2017. **8**: p. 14866.
51. Kodani, A., et al., *Centriolar satellites assemble centrosomal microcephaly proteins to recruit CDK2 and promote centriole duplication.* Elife, 2015. **4**.
52. Firat-Karalar, E.N., et al., *Proximity interactions among centrosome components identify regulators of centriole duplication.* Curr Biol, 2014. **24**(6): p. 664-70.
53. Fava, L.L., et al., *The PIDDosome activates p53 in response to supernumerary centrosomes.* Genes Dev, 2017. **31**(1): p. 34-45.
54. Burigotto, M., et al., *Centriolar distal appendages activate the centrosome-PIDDosome-p53 signalling axis via ANKRD26.* Embo j, 2021. **40**(4): p. e104844.
55. Sun, L., et al., *JFK, a Kelch domain-containing F-box protein, links the SCF complex to p53 regulation.* Proc Natl Acad Sci U S A, 2009. **106**(25): p. 10195-200.
56. Nishiyama, M., et al., *CHD8 suppresses p53-mediated apoptosis through histone H1 recruitment during early embryogenesis.* Nat Cell Biol, 2009. **11**(2): p. 172-82.
57. Sebti, S., et al., *BAT3 modulates p300-dependent acetylation of p53 and autophagy-related protein 7 (ATG7) during autophagy.* Proc Natl Acad Sci U S A, 2014. **111**(11): p. 4115-20.
58. Liu, L., et al., *p53 sites acetylated in vitro by PCAF and p300 are acetylated in vivo in response to DNA damage.* Mol Cell Biol, 1999. **19**(2): p. 1202-9.
59. Li, Z., et al., *The OncoPPi network of cancer-focused protein-protein interactions to inform biological insights and therapeutic strategies.* Nat Commun, 2017. **8**: p. 14356.
60. Tohkin, M., et al., *Aryl hydrocarbon receptor is required for p300-mediated induction of DNA synthesis by adenovirus E1A.* Mol Pharmacol, 2000. **58**(4): p. 845-51.
61. Tong, Q., et al., *MnTE-2-PyP reduces prostate cancer growth and metastasis by suppressing p300 activity and p300/HIF-1/CREB binding to the promoter region of the PAI-1 gene.* Free Radic Biol Med, 2016. **94**: p. 185-94.
62. Gupta, G.D., et al., *A Dynamic Protein Interaction Landscape of the Human Centrosome-Cilium Interface.* Cell, 2015. **163**(6): p. 1484-99.

63. Hatakeyama, S., *TRIM Family Proteins: Roles in Autophagy, Immunity, and Carcinogenesis.* Trends Biochem Sci, 2017. **42**(4): p. 297-311.
64. Soucy, T.A., et al., *An inhibitor of NEDD8-activating enzyme as a new approach to treat cancer.* Nature, 2009. **458**(7239): p. 732-6.
65. Sillibourne, J.E., et al., *Autophosphorylation of polo-like kinase 4 and its role in centriole duplication.* Mol Biol Cell, 2010. **21**(4): p. 547-61.
66. Lambrus, B.G. and A.J. Holland, *A New Mode of Mitotic Surveillance.* Trends Cell Biol, 2017. **27**(5): p. 314-321.
67. Uetake, Y. and G. Sluder, *Prolonged prometaphase blocks daughter cell proliferation despite normal completion of mitosis.* Curr Biol, 2010. **20**(18): p. 1666-71.
68. Yau, R. and M. Rape, *The increasing complexity of the ubiquitin code.* Nat Cell Biol, 2016. **18**(6): p. 579-86.
69. Xie, H., et al., *ROS/NF-kappaB Signaling Pathway-Mediated Transcriptional Activation of TRIM37 Promotes HBV-Associated Hepatic Fibrosis.* Mol Ther Nucleic Acids, 2020. **22**: p. 114-123.
70. Li, Y., et al., *Tripartite motif-containing 37 (TRIM37) promotes the aggressiveness of non-small-cell lung cancer cells by activating the NF-kappaB pathway.* J Pathol, 2018. **246**(3): p. 366-378.
71. Wu, G., et al., *An ATM/TRIM37/NEMO Axis Counteracts Genotoxicity by Activating Nuclear-to-Cytoplasmic NF-kappaB Signaling.* Cancer Res, 2018. **78**(22): p. 6399-6412.
72. Wang, W., et al., *TRIM37 deficiency induces autophagy through deregulating the MTORC1-TFEB axis.* Autophagy, 2018. **14**(9): p. 1574-1585.
73. Denu, R.A., et al., *Centrosome Amplification in Cancer Disrupts Autophagy and Sensitizes to Autophagy Inhibition.* Mol Cancer Res, 2020. **18**(1): p. 33-45.
74. Lei, Q., et al., *YLT-11, a novel PLK4 inhibitor, inhibits human breast cancer growth via inducing maladjusted centriole duplication and mitotic defect.* Cell Death Dis, 2018. **9**(11): p. 1066.
75. Holland, A.J. and D.W. Cleveland, *Polo-like kinase 4 inhibition: a strategy for cancer therapy?* Cancer Cell, 2014. **26**(2): p. 151-3.
76. Kodani, A., et al., *SFI1 promotes centriole duplication by recruiting USP9X to stabilize the microcephaly protein STIL.* J Cell Biol, 2019. **218**(7): p. 2185-2197.
77. Zimmermann, M., et al., *CRISPR screens identify genomic ribonucleotides as a source of PARP-trapping lesions.* Nature, 2018. **559**(7713): p. 285-289.
78. Olivieri, M. and D. Durocher, *Genome-scale chemogenomic CRISPR screens in human cells using the TKOv3 library.* STAR Protoc, 2021. **2**(1): p. 100321.
79. Shannon, P., et al., *Cytoscape: a software environment for integrated models of biomolecular interaction networks.* Genome Res, 2003. **13**(11): p. 2498-504.
80. Bindea, G., et al., *ClueGO: a Cytoscape plug-in to decipher functionally grouped gene ontology and pathway annotation networks.* Bioinformatics, 2009. **25**(8): p. 1091-3.
81. Sanjana, N.E., O. Shalem, and F. Zhang, *Improved vectors and genome-wide libraries for CRISPR screening.* Nat Methods, 2014. **11**(8): p. 783-784.
82. Brinkman, E.K., et al., *Easy quantitative assessment of genome editing by sequence trace decomposition.* Nucleic Acids Res, 2014. **42**(22): p. e168.
83. McQuin, C., et al., *CellProfiler 3.0: Next-generation image processing for biology.* PLoS Biol, 2018. **16**(7): p. e2005970.

84. Mojarad, B.A., et al., *CEP19 cooperates with FOP and CEP350 to drive early steps in the ciliogenesis programme.* Open Biol, 2017. **7**(6).
85. Schneider, C.A., W.S. Rasband, and K.W. Eliceiri, *NIH Image to ImageJ: 25 years of image analysis.* Nat Methods, 2012. **9**(7): p. 671-5.
86. Arganda-Carreras, I., et al., *Trainable Weka Segmentation: a machine learning tool for microscopy pixel classification.* Bioinformatics, 2017. **33**(15): p. 2424-2426.

FIGURE LEGENDS

Figure 1. Concentration-dependent effect of centrinone B on centriole number. (A) RPE-1 cells were serially grown for 12 days and treated as indicated with centrinone B. Relative cell number compared to a DMSO-treated control was determined and plotted. Means ± SEM shown (n = 3). **(B)** RPE-1 cells were treated with DMSO or 200 or 500 nM centrinone B for 4 days and prepared for Western blot probing for the indicated proteins. Ponceau S indicates total protein. **(C)** RPE-1 cells were treated as in (B), fixed for immunofluorescence and stained for the indicated protein. Inset magnified 3x. **(D)** Cells as treated in (C) were analyzed for nuclear p53. Means ± SEM shown (n = 3, N > 100). **(E)** Cells as treated in (C) were stained for the centriole marker CEP135 and foci counted. Means ± SEM shown (n = 3, N > 100).

Figure 2. CRISPR/Cas9 screen to interrogate response to abnormal centrosome number. (A) Schematic outlining our screening procedures. RPE-1 expressing Cas9 were infected with the TKOv1 genome-wide CRISPR sgRNA library and subsequently grown for 21 days in the presence of DMSO, 200 nM centrinone B, 500 nM centrinone B or 600 nM Nutlin-3a. The sgRNA distribution in each pool of cells was determined using NGS and analyzed using MAGeCK. **(B)** The significant hits ($p < 0.05$) from all screens were combined to form a network. The screening conditions are represented as hubs. The general automated yFiles organic layout from Cytoscape was preserved while individual nodes were manually arranged to facilitate visualization. Selected complexes and protein nodes are labeled and highlighted.

Figure 3. TRIM37 is a centrosome-associated protein. (A) RPE-1 cells were stably infected with virus directing the expression of Cas9 and one of two sgRNAs against TRIM37 or empty vector. Selected cells were treated with DMSO, or 200 nM or 500 nM centrinone B for 4 days, fixed and stained for CEP135 and foci counted. A representative of two independent experiments is shown. **(B)** Cells from (A) were also processed for Western blotting using the indicated antibodies. FL – full length. p60 – p60 fragment. Ponceau S indicates total protein. **(C) and (D)** Asynchronous RPE-1 cells were fixed and stained with the indicated antibodies. **(E)** RPE-1 *TRIM37*$^{-/-}$ cells stably expressing FB-TRIM37 were fixed, stained with the indicated antibody and imaged using 3D-SIM.

Figure 4. TRIM37 E3-independent activity is required for growth arrest (A) Schematic representation of TRIM37 domain structure. **(B)** RPE-1 *TRIM37*$^{-/-}$ cells were transfected to express Myc-PLK4 and FB or the indicated FB-TRIM37 fusion protein (top). Cells were lysed and subjected to anti-FLAG immunoprecipitation. Input and immunoprecipitates were analyzed by immunoblotting with the indicated antibodies. Ponceau S indicates total protein. * indicates position of FLAG-Cas9 **(C)** WT and *TRIM37*$^{-/-}$ RPE-1 cells stably expressing FB or the indicated FB-TRIM37 fusion protein were seeded for clonogenic survival assays and grown in DMSO or the indicated concentration of centrinone B for 14 days. Colony size after staining was quantified. Means ± SD shown (n = 2). **(D)** WT RPE-1, *TRIM37*$^{-/-}$ and *TRIM37*$^{-/-}$ cells expressing FB or the indicated FB-TRIM37 construct were seeded for clonogenic assays and grown in DMSO or the indicated concentration of centrinone B for 14 days. Colony density was quantified and growth compared to that in DMSO determined. Means ± SD shown (n = 3). **(E)** WT, *TP53*$^{-/-}$ and *TRIM37*$^{-/-}$ RPE-1 cells were infected to stably express tetracycline-inducible PLK4-3xFLAG. Cells were seeded for a clonogenic assay and grown in the presence or absence of

1μg/mL tetracycline (tet) for 14 days. Colony density was quantified and growth in the presence of tetracycline compared to growth in its absence. Means ± SD shown (n = 3).

Figure 5. TRIM37 displays E3-dependent and -independent activities (A) WT or *TRIM37*$^{-/-}$ RPE-1 cells were grown for 3 days in DMSO or the indicated concentration of centrinone B. SiR-DNA was added for 2 h before live imaging for 24 h. The time between nuclear envelope breakdown and telophase was determined for at least 55 cells per condition. Pooled results from two independent experiments are shown. Boxplots indicate median, 25% and 75% quartiles and the whiskers extend 1.5x the interquartile range. Points indicate data falling outside this range. *p*-values refer to WT compared to *TRIM37*$^{-/-}$ and were calculated by Wilcox test at each centrinone B concentration. **(B)** Statistical analysis of data from (A). Samples from the indicated cell line were analyzed using a Kruskal-Wallace ANOVA followed by a post-hoc Dunn test. **(C)** RPE-1 *TRIM37*$^{-/-}$ cells stably expressing the indicated FB fusion protein were treated and analyzed as in (A). **(D)** Statistical analysis of data from (C). Samples from the indicated cell line were analyzed using a Kruskal-Wallace ANOVA followed by a post hoc Dunn test. **(E)** Asynchronous WT or *TRIM37*$^{-/-}$ RPE-1 cells stably expressing the indicated fusion protein were fixed and stained for the indicated protein. Arrowheads indicate extra-centrosomal accumulations. **(F)** and **(G)** WT or *TRIM37*$^{-/-}$ RPE-1 cells stably expressing the indicated protein were grown in 500 nM centrinone B for 4 days, fixed and immunostained for PCNT, CEP192 and CEP120 or CEP97. For (F), mitotic phase was determined from DAPI staining. For (G), the percentage of mitotic cells displaying a pseudo-bipolar MTOC arrangement was counted. Means ± SD shown (n = 2, N = 50). Cell lines coloured in red indicate functional growth arrest activity.

Figure 6. TRIM37 negatively regulates centriole and centrosome proteins. (A) Asynchronous WT and clonal *TRIM37*$^{-/-}$ RPE-1 cells were analyzed by immunoblot for the indicated proteins. Ponceau S indicates total protein. **(B)** Asynchronous clonal *TRIM37*$^{-/-}$ RPE-1 cells stably expressing the indicated protein (top) were analyzed by Western blot with the indicated antibody (right). **(C)** WT RPE-1 cells expressing tetracycline-inducible TRIM37-3xFLAG (WT) or TRIM37 C18R-3xFLAG (C18R) were induced with doxycycline for 0, 4, 8, 48 or 72 h. At each time point, extracts were prepared and analyzed by Western blot for the indicated protein (right). Ponceau S indicates equal loading. CEP192 abundance was quantified (bottom) Mean ± SD shown (n = 3) **(D)** Cells from (C) were also fixed and immunostained for the indicated proteins. The total centrosomal intensity of the indicated proteins was determined using CellProfiler. Intensity values normalized to 0 h for both replicates are shown (grey circles, n = 2, N = 30). Means from each replicate are indicated by a coloured bar.

Figure 7. TRIM37 promotes PLK4 phosphorylation in an E3-dependent manner. (A) HEK293T cells transfected to express Myc-PLK4 and the indicated protein (top) were grown overnight and subsequently treated with DMSO or MLN4924 for 22 h and MG132 for 4 h. Cell extracts were prepared and probed by Western blot using the indicated antibodies. Ponceau S indicates total protein. **(B)** HEK293T cells were transfected to express Myc-PLK4, HA-Ub and the indicated protein (top). Cells were harvested after 48 h and subjected to immunoprecipitation using anti-Myc antibodies. Input and immunoprecipitates were analyzed by immunoblotting for PLK4 and HA-Ub. Ponceau S indicates total protein. **(C)** HEK293T cells were transfected to express Myc-PLK4 and the indicated protein (top) for 48 h. MG132 was added for the last 4 h. Lysates were mock treated or incubated with λ-phosphatase and subsequently subjected to immunoblot for PLK4. **(D)** HEK293T cells were transfected to express Myc-PLK4 and T7-

TRIM37 Δ505-709 for 48 h. Cells were treated with the indicated inhibitor (top) for 3 or 6 h and analyzed by immunoblot for PLK4. Ponceau S indicates total protein.

SUPPLEMENTAL FIGURE LEGENDS

Figure 1 – figure supplement 1. Centrinone B induces growth arrest at multiple concentrations. (A) RPE-1 cells were treated with DMSO, or 200 or 500 nM centrinone B for 4 days. Fixed cells were immunostained for p21 and the percent p21-positive cells was quantified using CellProfiler. The mean ± SD is shown (n = 2, N > 100). **(B)** RPE-1 cells treated as in (A) were fixed, stained with propidium iodide and subjected to flow cytometry to analyze DNA content. The results from a representative experiment are shown. **(C)** RPE-1 cells treated with DMSO or 200 nM centrinone B for 4 days were fixed and stained for the indicated proteins. Two representative images per condition are shown.

Figure 2 – figure supplement 1. Bioinformatic analysis of CRISPR/Cas9 screens. (A-D) Biological process enrichment from significant genes scoring in each screen using RPE-1 cells. Screen type indicated in each figure. **(E)** Zoom of Figure 2B to show positions of AHR, ARNT and AIP. **(F)** Protein-protein interaction network of genes identified as suppressors in the Nutlin-3a screen.

Figure 2 – figure supplement 2. Comparison of PLK4 screens. (A-G) Venn diagrams showing the overlap among the screens indicated in each panel. Genes from selected overlap regions are shown. **(G)** All 22 genes in the overlap were identified using A375 cells. Genes coloured in red were also identified using RPE-1 cells.

Figure 3 – figure supplement 1. Characterization of TRIM37 gene disrupted lines. (A) The indicated cell lines were analyzed by Western blotting for TRIM37. Ponceau S indicates total protein. **(B)** Results from Synthego ICE analysis of clonal RPE-1 *TRIM37*$^{-/-}$ gene disruption. WT sequence is shown at bottom. sgRNA sequence is underlined and PAM coloured red. Vertical line indicates predicted Cas9 cleavage site. The deconvolved sequences indicate alleles with 1 and 2 nucleotide deletions.

Figure 4 – figure supplement 1. Characterization of TRIM37 rescue lines. (A) RPE-1 cells were transfected with plasmids to express Myc-PLK4 and the indicated protein (top). After 24 h cells were harvested and extracts were subjected to imunoprecipitation using anti-FLAG antibodies. Input and immunoprecipitates were analyzed by Western blot for FLAG and PLK4. Ponceau S indicates total protein. **(B)** WT RPE-1 and a clonal *TRIM37*$^{-/-}$ line stably expressing the indicated fusion proteins were harvested and analyzed by Western blotting for the indicated FLAG-tagged proteins. Ponceau S indicates total protein. **(C)** WT and *TRIM37*$^{-/-}$ RPE-1 cells stably expressing the indicated FB-TRIM37 fusion protein were seeded for clonogenic assays and grown in DMSO or the indicated concentration of centrinone B for 14 days. Colony size after staining was quantified. Means ± SEM shown (n = 2). **(D)** WT RPE-1 and a pooled RPE-1 *TRIM37*$^{-/-}$ line stably expressing the indicated fusion protein were harvested and analyzed by Western blotting for the indicated FLAG-tagged proteins. Ponceau S indicates total protein. **(E)** Cells from (D) were also fixed and stained to detect BirA, CEP135 and CEP120. **(F)** WT A375 and *TRIM37*$^{-/-}$ pools stably expressing the indicated protein were harvested and analyzed by Western blotting for the indicated FLAG-tagged proteins. Ponceau S indicates total protein.. **(G)** WT A375, *TRIM37*$^{-/-}$ and *TRIM37*$^{-/-}$ cells expressing FLAG-BirA or the indicated FB-TRIM37 construct were seeded for clonogenic assays and grown in DMSO or the indicated concentration

of centrinone B for 10 days. Colony density was quantified and growth compared to that in DMSO determined. Means ± SD shown (n = 3) **(H)** RPE-1 (top) or A375 (bottom), WT and *TRIM37*$^{-/-}$ cells were grown in DMSO or the indicated concentration of centrinone B (nM) for 4 days, fixed and stained for CEP135. The number of CEP135 foci in at least 100 cells were counted per condition. Results from a single experiment shown.

Figure 5 – figure supplement 1. Extracentrosomal accumulations of centriole components. (A) RPE-1 *TRIM37*$^{-/-}$ cells were fixed and stained for the indicated proteins. **(B)** RPE-1 *TRIM37*$^{-/-}$ cells expressing tetracycline-inducible PLK4-3xFLAG were induced for 0 (UN), 3 or 6 h, fixed and stained for the indicated proteins. **(C)** Cells from (A) were fixed and stained for the indicated proteins. Mitotic cells are shown; prophase, anaphase, telophase (left to right). Arrowhead indicates extracentrosomal accumulation of CNTROB that co-localizes with CEP192. **(D)** RPE-1 *TRIM37*$^{-/-}$ cells were treated with 500 nM centrinone B for 4 days, fixed and stained for the indicated proteins. A representative mitotic cell is shown. Note that the dispersed localization of CEP192 is indicative of an acentrosomal cell. **(E)** Clonal RPE-1 *TRIM37*$^{-/-}$ cells stably expressing FB or the indicated FB-TRIM37 fusion protein were fixed and stained for BirA. **(F)** Clonal RPE-1 *TRIM37*$^{-/-}$ cells stably expressing the indicated FB-TRIM37 fusion protein were fixed and stained for the indicated protein.

Figure 5 – figure supplement 2. Ectopic accumulation of PCM components. (A) and (B) RPE-1 *TRIM37*$^{-/-}$ pools stably expressing FB or the indicated FB-TRIM37 fusion protein were grown in 500 nM centrinone B for 4 days, fixed and stained for the indicated proteins. Images in (A) provide examples of bi-polar arrangement of ectopic PCM proteins. Images in (B) provide examples of monopolar arrangement of PCM around a single centriole (top) and the absence of ectopic PCM in an acentriolar mitotic cell (bottom).

Figure 6 – figure supplement 1. TRIM37 negatively regulates centrosome accumulation of PCM and centriole proteins. (A) and (B) RPE-1 cells expressing tetracycline-inducible TRIM37-3xFLAG or TRIM37 C18R-3xFLAG were induced with tetracycline for 0, 4, 8, 48 or 72 h, fixed and stained for the indicated proteins. The centrosomal intensities (A) and areas (B) were determined using CellProfiler. Normalized values for two independent replicates are shown (grey circles, N = 30 metaphase cells). Means from each replicate are indicated.

SUPPLEMENTAL FILES

Table S1. Summary of screening data. (excel file)

Table S2. Gene enrichment details for RPE-1 screens. (excel file)

Table S3. Reagents used in this study. (excel file)

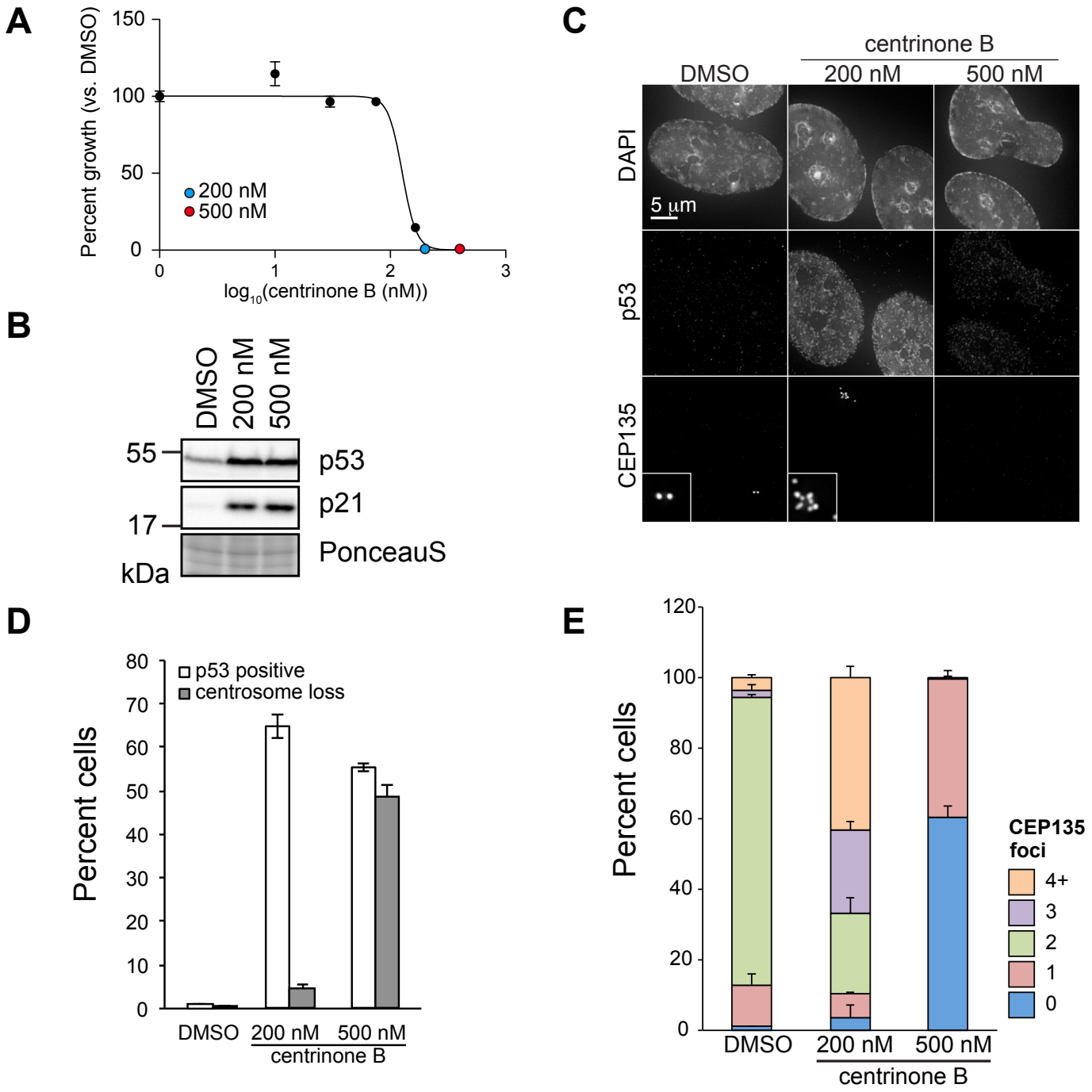

Figure 1

Tkach JM *et al.*

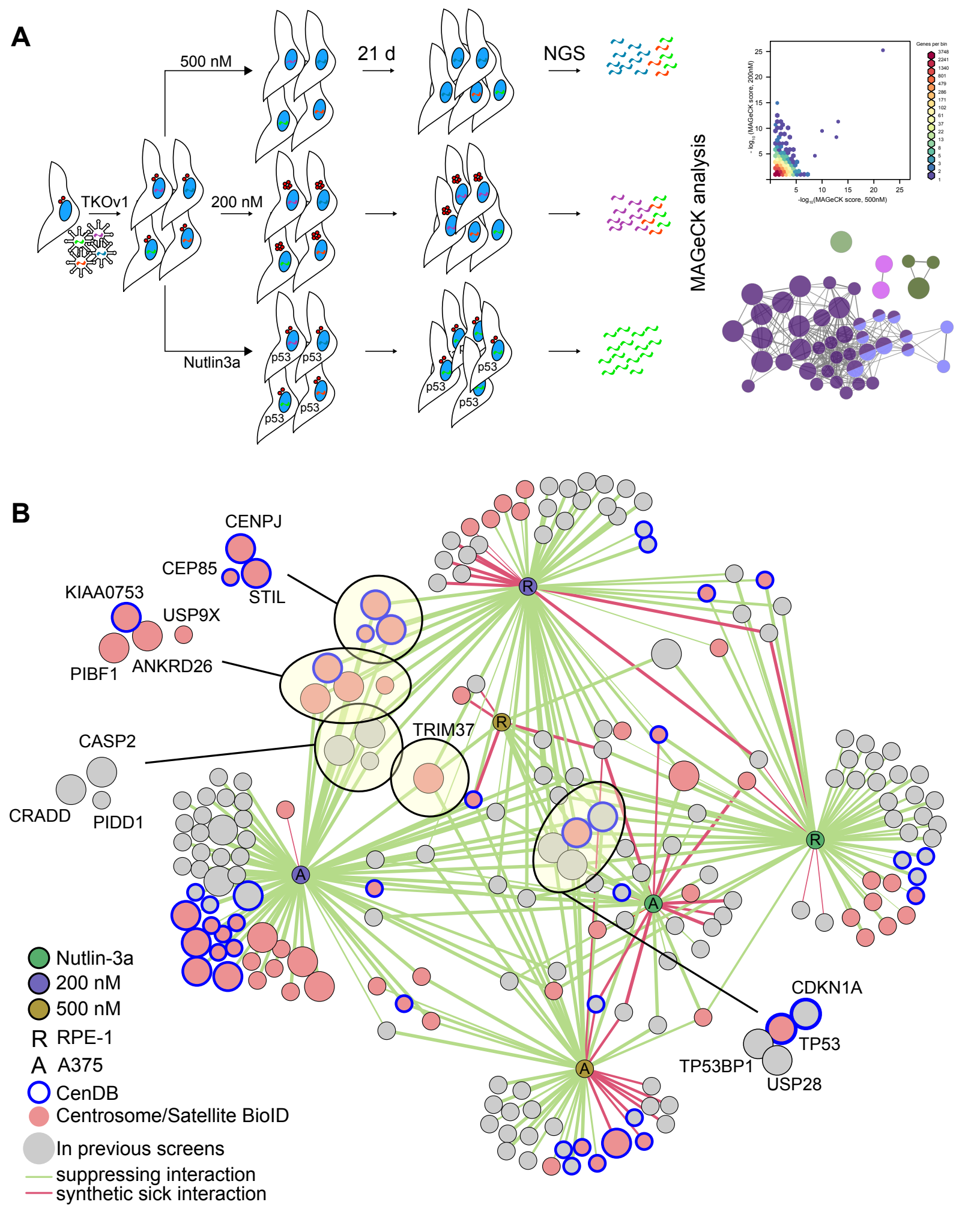

Figure 2

Tkach JM *et al.*

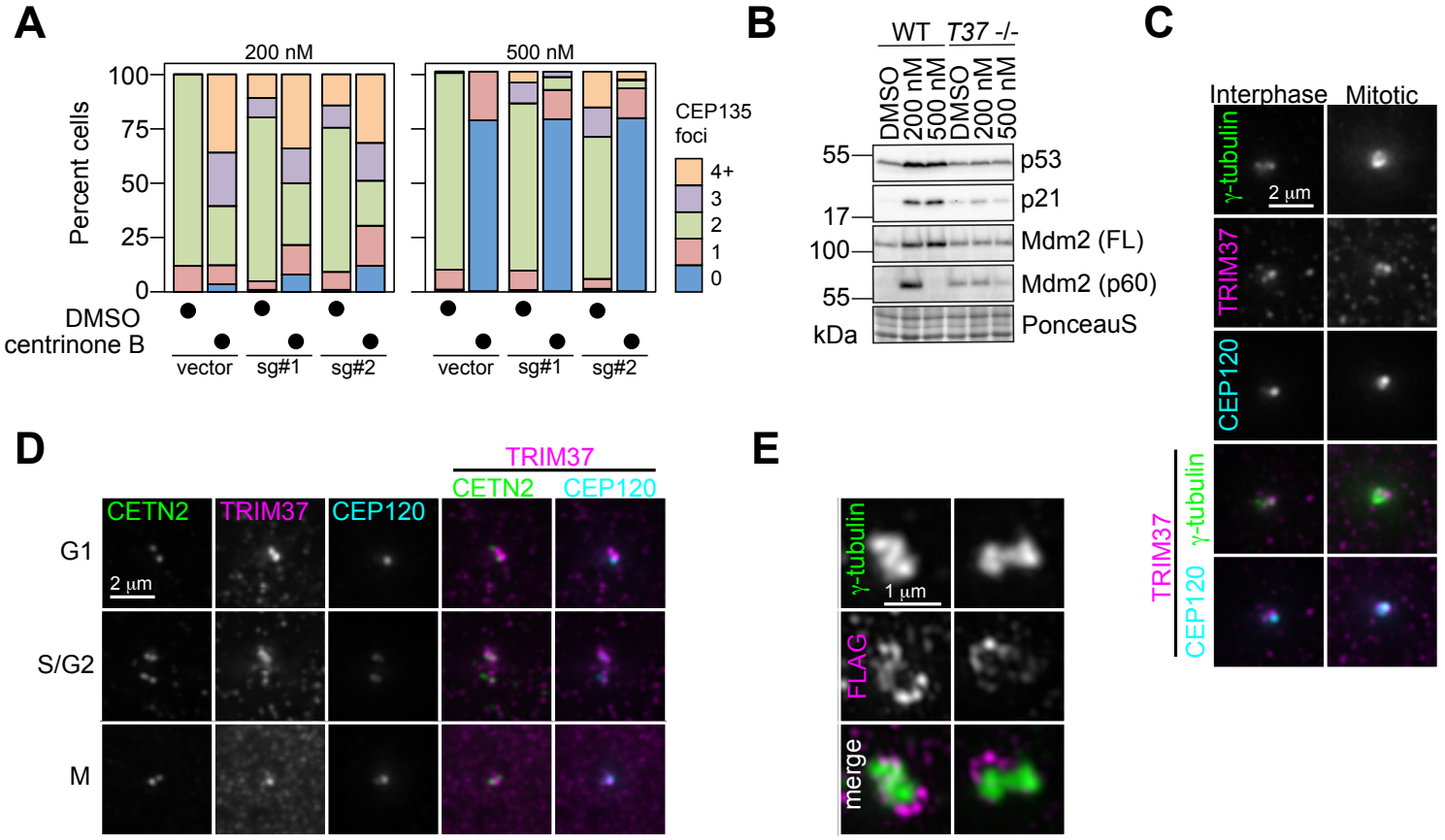

Figure 3

Tkach JM *et al.*

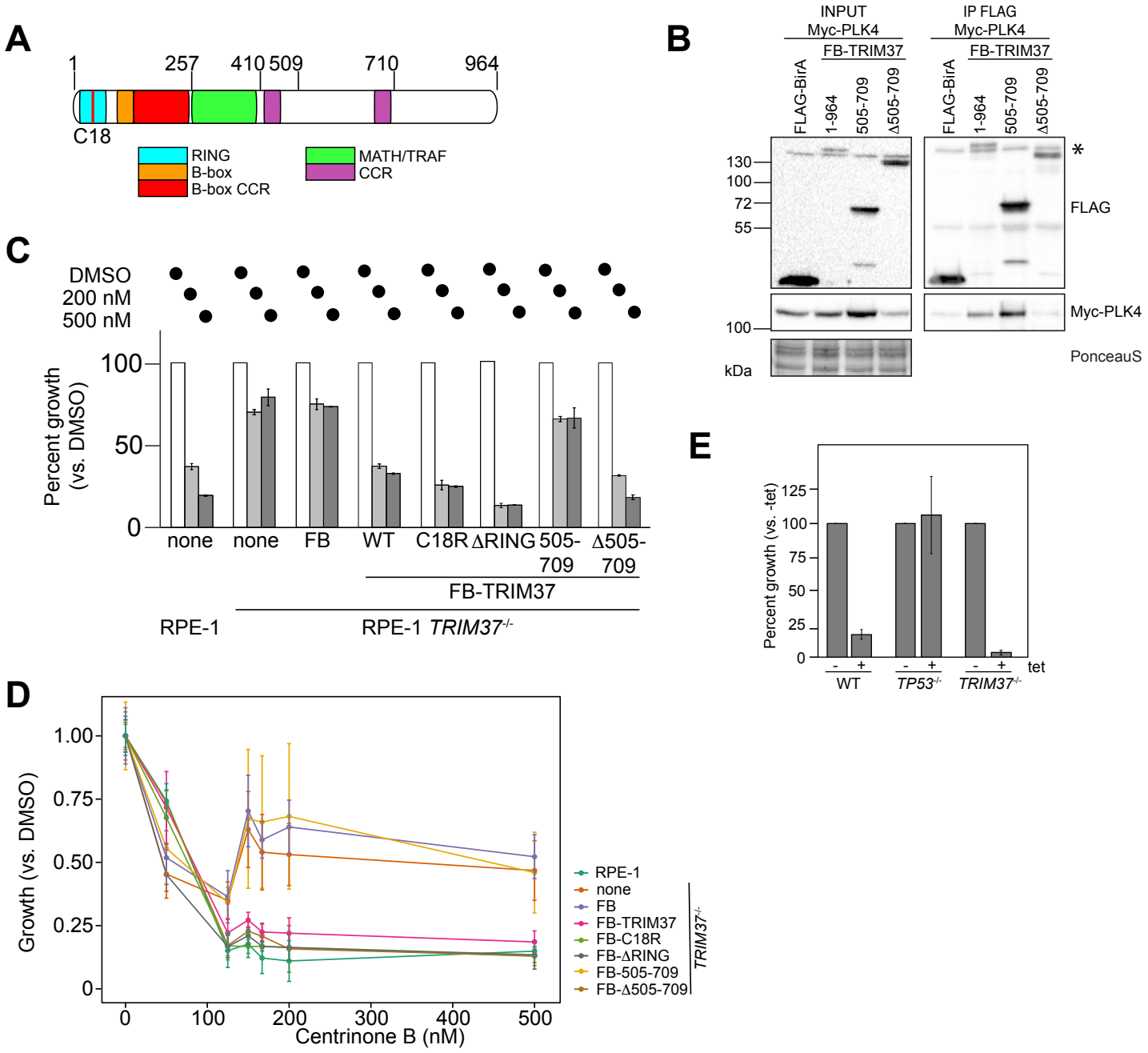

Figure 4

Tkach JM *et al.*

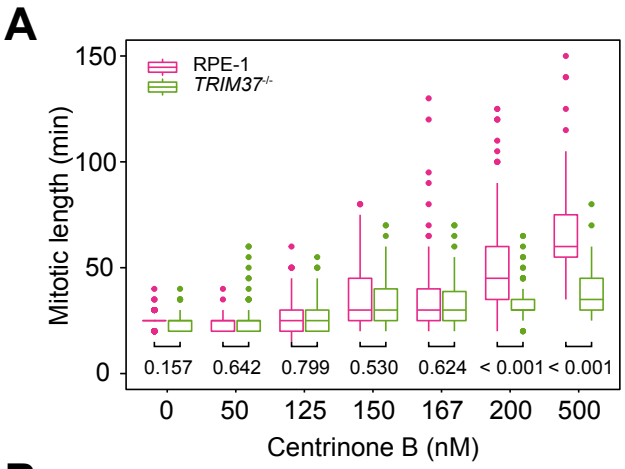

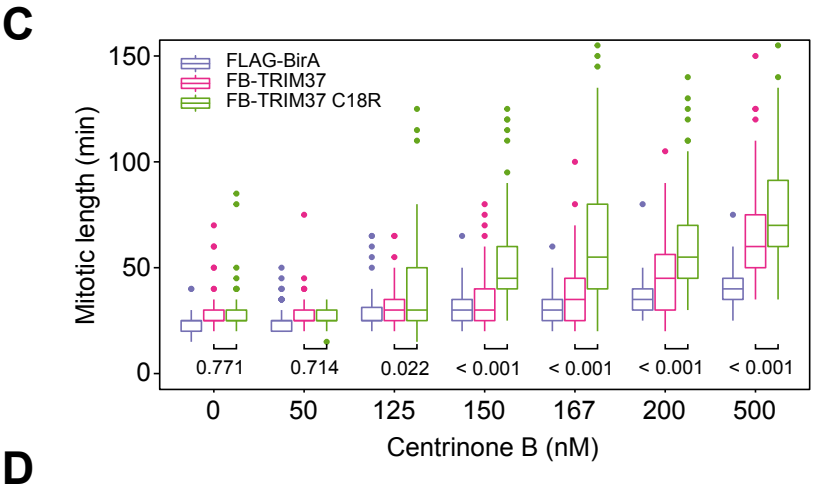

B

	WT		*TRIM37*$^{-/-}$ pool	
Cent. B (nM)	Length (min)	*p*-value	Length (min)	*p*-value
DMSO	25	NA	25	NA
50	25	0.159	25	0.248
125	25	0.081	25	0.010
150	30	9.56×10^{-13}	30	3.42×10^{-13}
167	30	1.73×10^{-12}	30	1.04×10^{-12}
200	45	1.20×10^{-36}	30	5.17×10^{-17}
500	60	4.29×10^{-62}	30	6.47×10^{-30}

D

	FLAG-BirA		FB-TRIM37		FB-TRIM37 C18R	
Cent. B (nM)	Length (min)	*p*-value	Length (min)	*p*-value	Length (min)	*p*-value
DMSO	25	NA	25	NA	25	NA
50	25	0.225	25	0.191	25	0.101
125	25	2.97×10^{-6}	30	0.007	30	7.29×10^{-5}
150	30	2.22×10^{-16}	30	1.51×10^{-5}	45	2.20×10^{-16}
167	30	1.77×10^{-11}	35	4.88×10^{-6}	55	5.70×10^{-25}
200	35	5.24×10^{-22}	45	3.48×10^{-16}	55	5.02×10^{-26}
500	40	1.76×10^{-37}	60	3.70×10^{-39}	70	6.77×10^{-41}

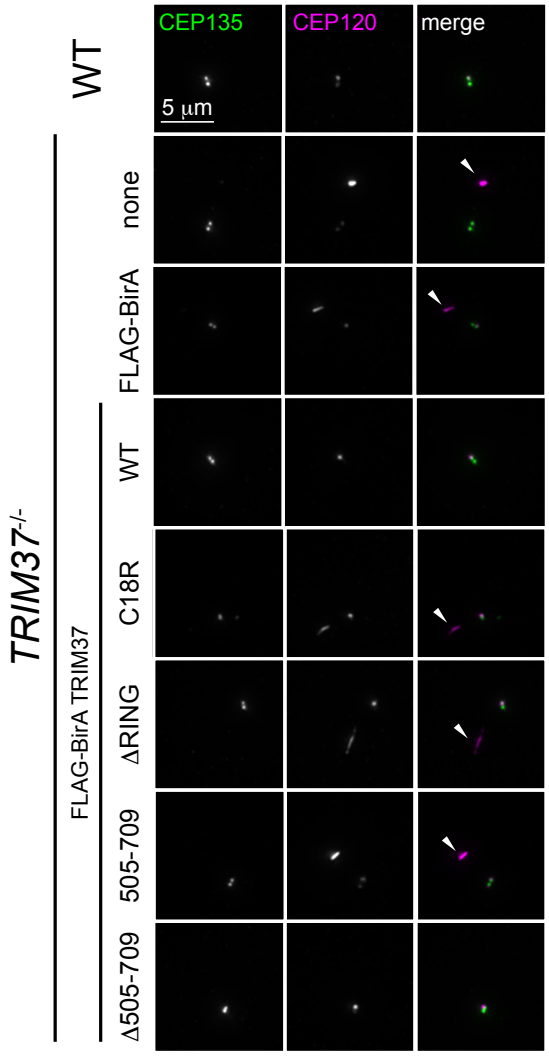

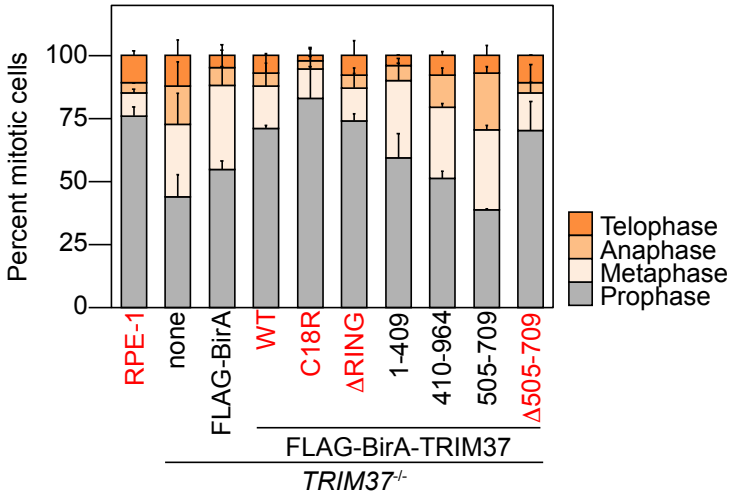

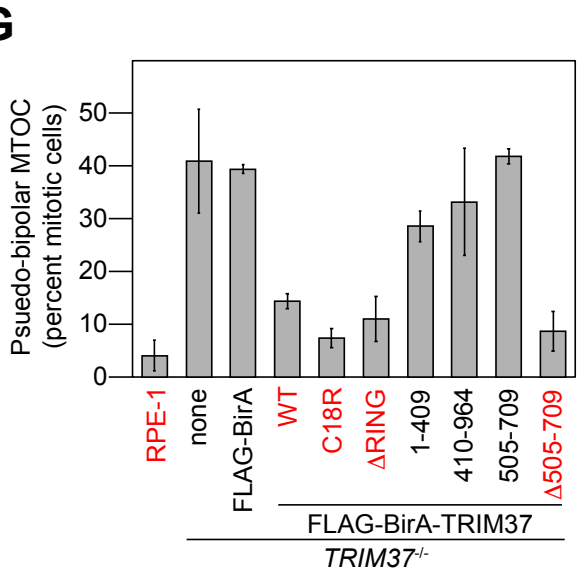

Figure 5

Tkach JM *et al.*

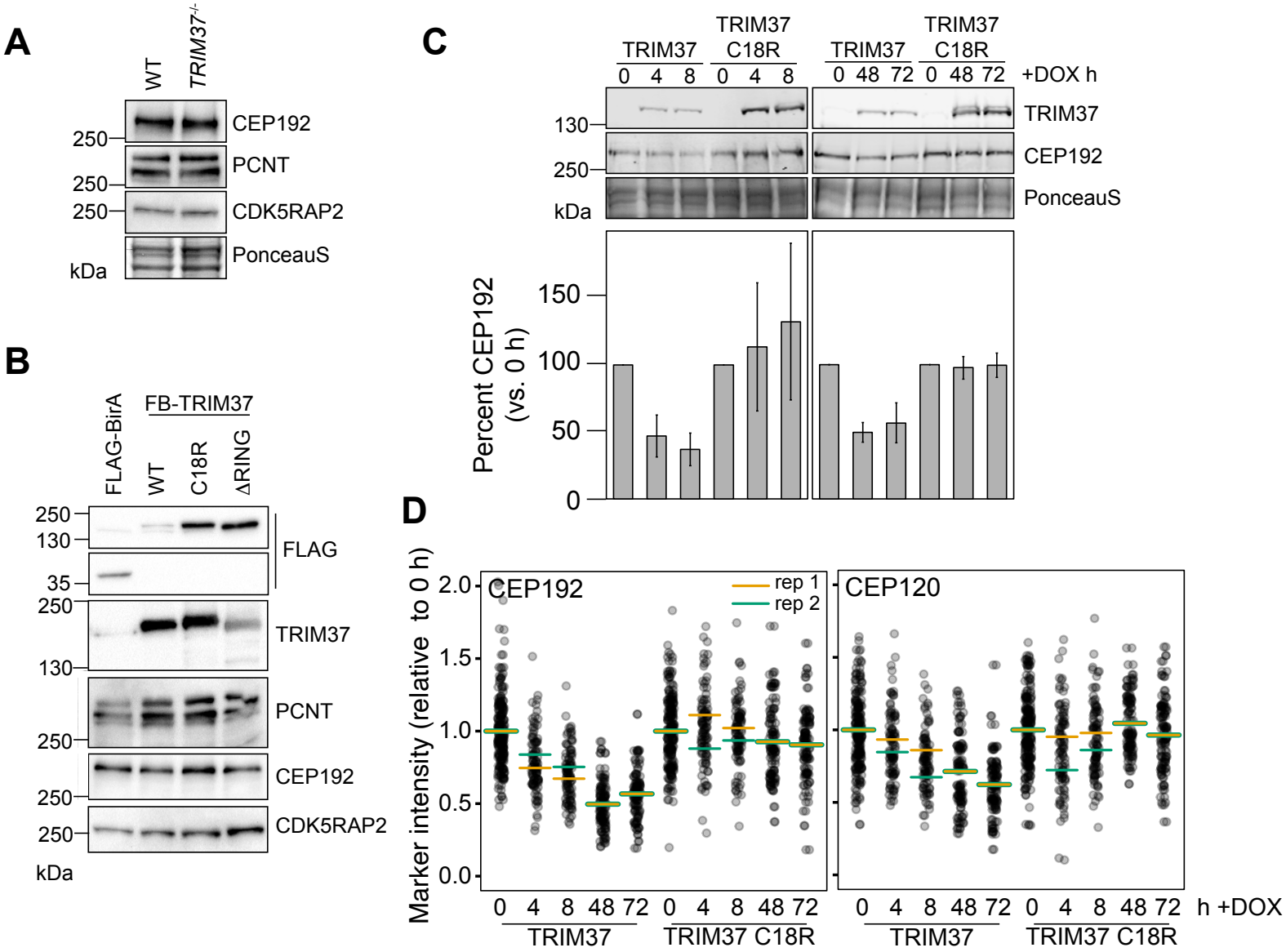

Figure 6

Tkach JM *et al.*

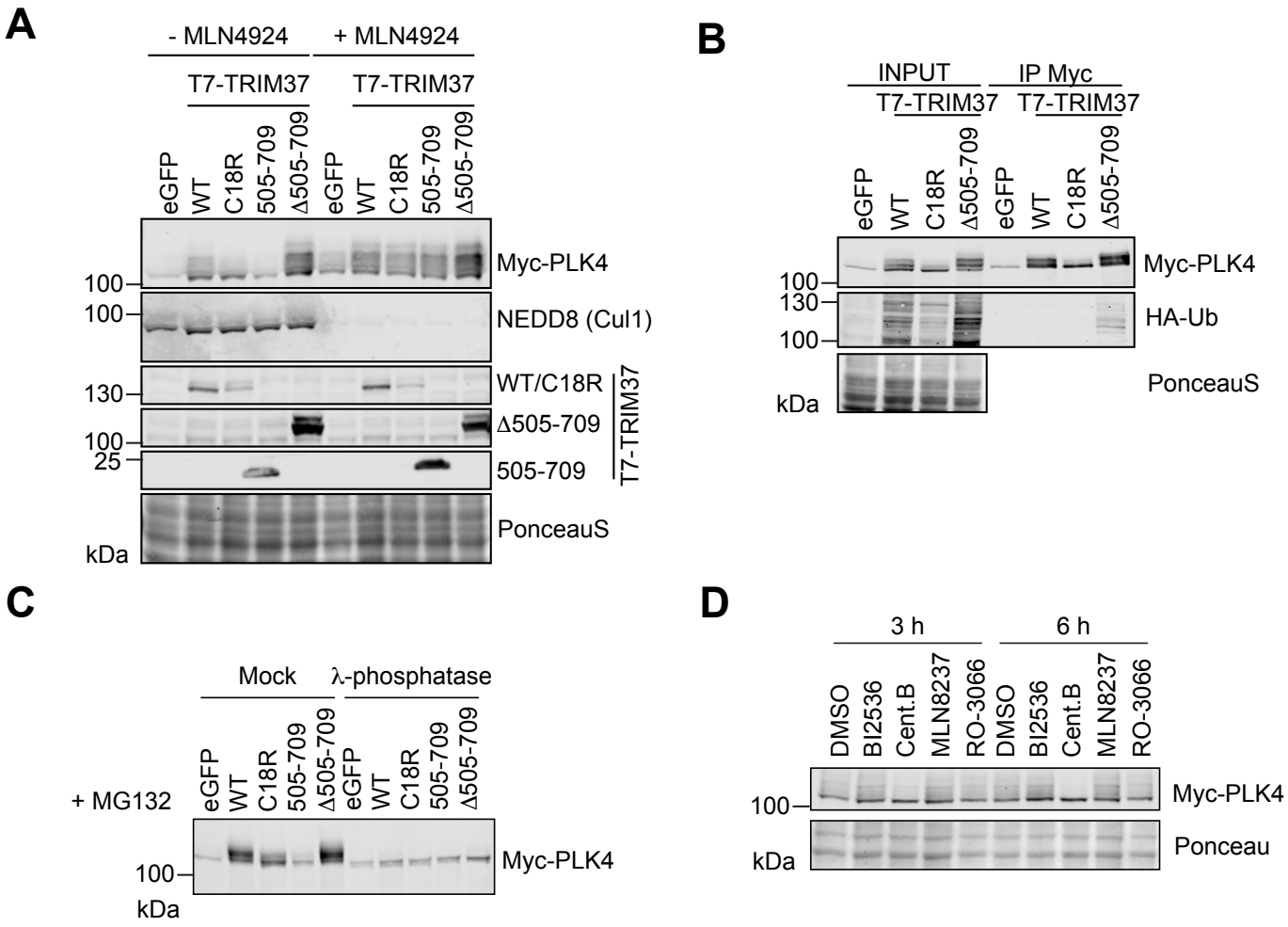

Figure 7

Tkach JM *et al.*

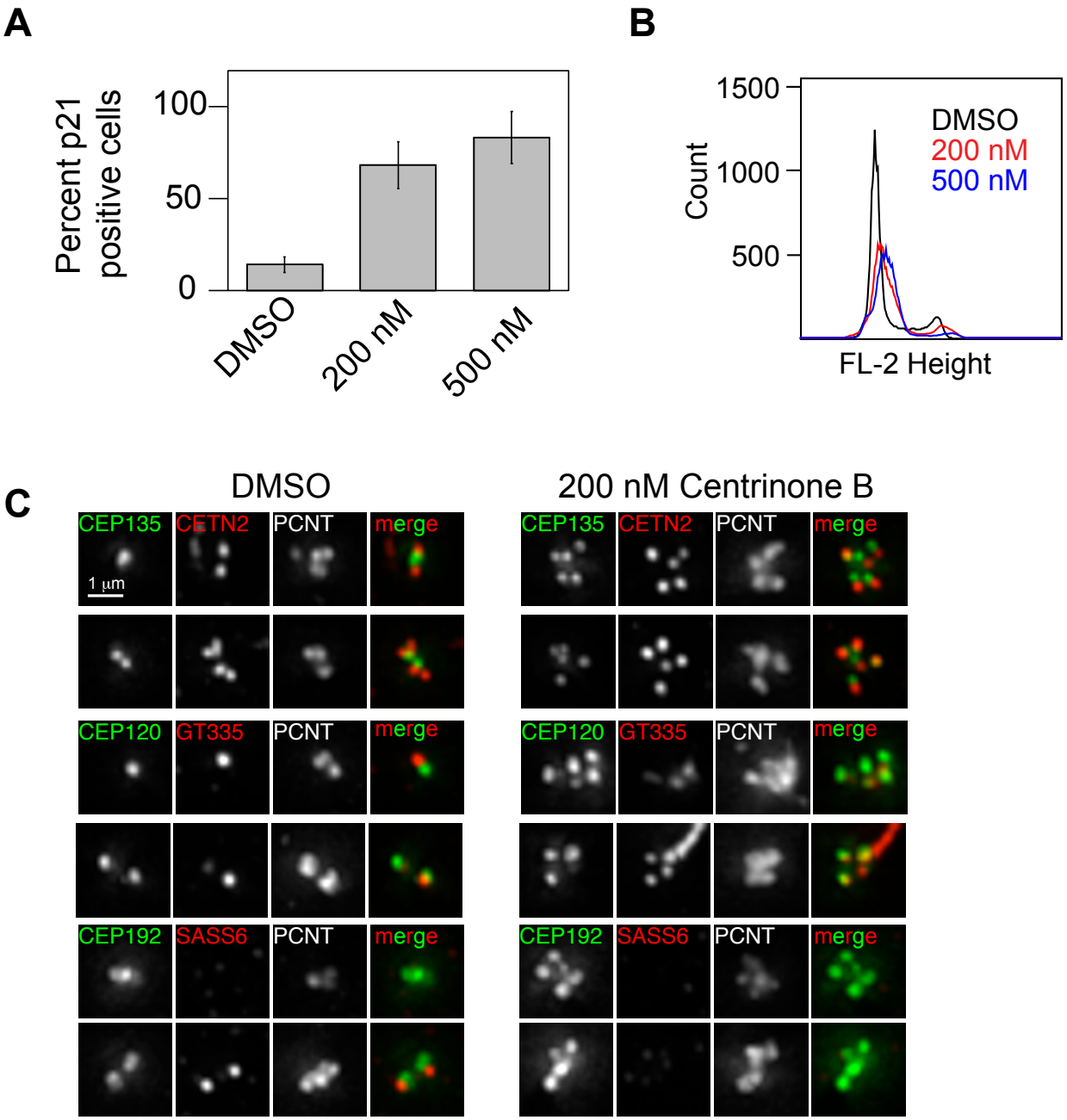

Figure 1 - figure supplement 1

Tkach JM *et al.*

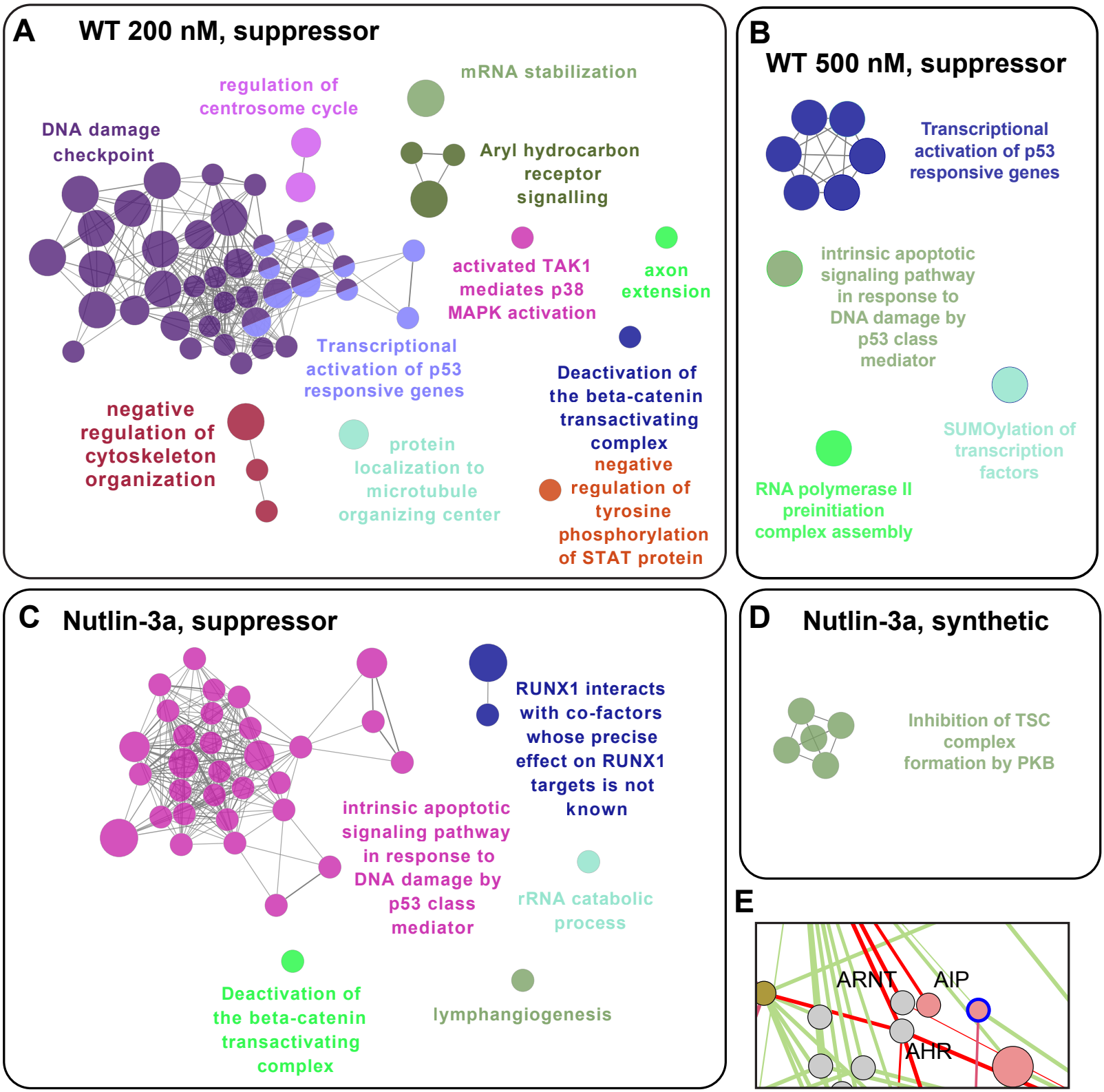

Figure 2 - figure supplement 1

Tkach JM *et al.*

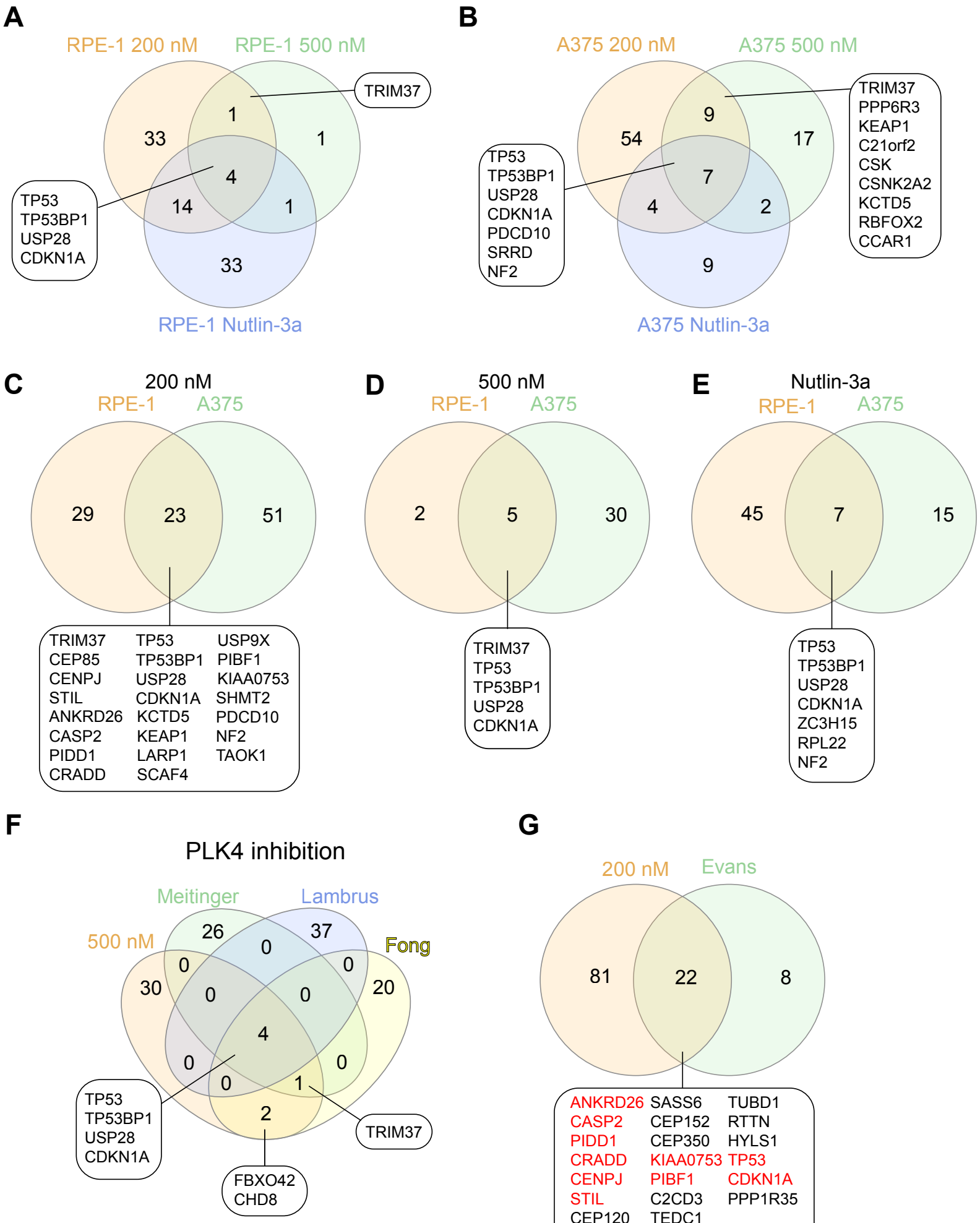

Figure 2 - figure supplement 2

Tkach JM *et al.*

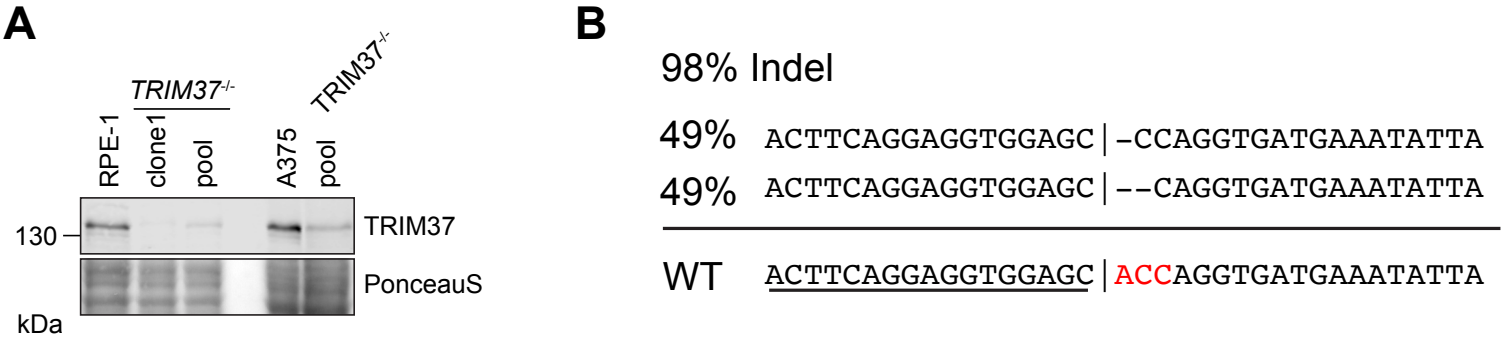

Figure 3 - figure supplement 1

Tkach JM *et al.*

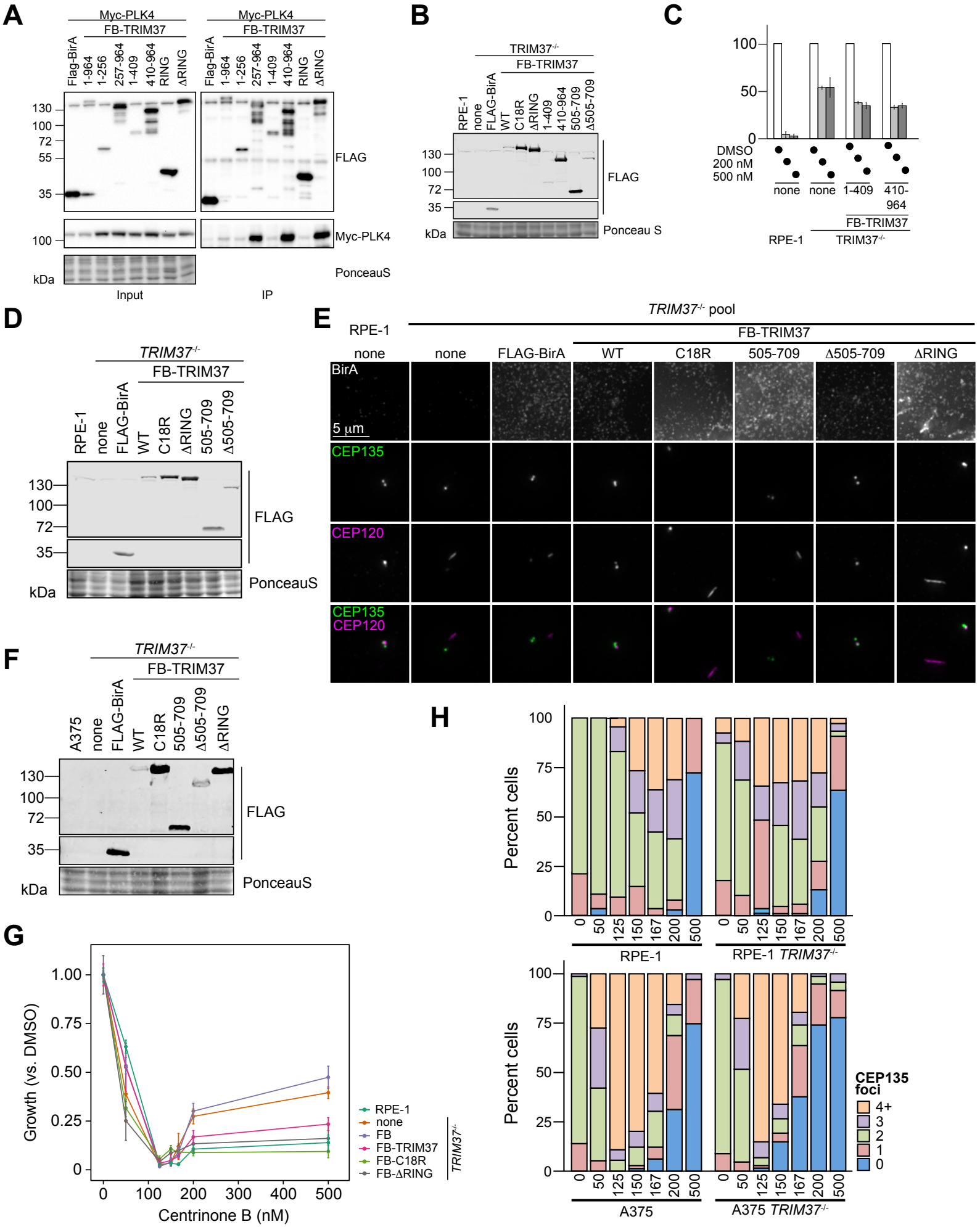

Figure 4 - figure supplement 1

Tkach JM *et al.*

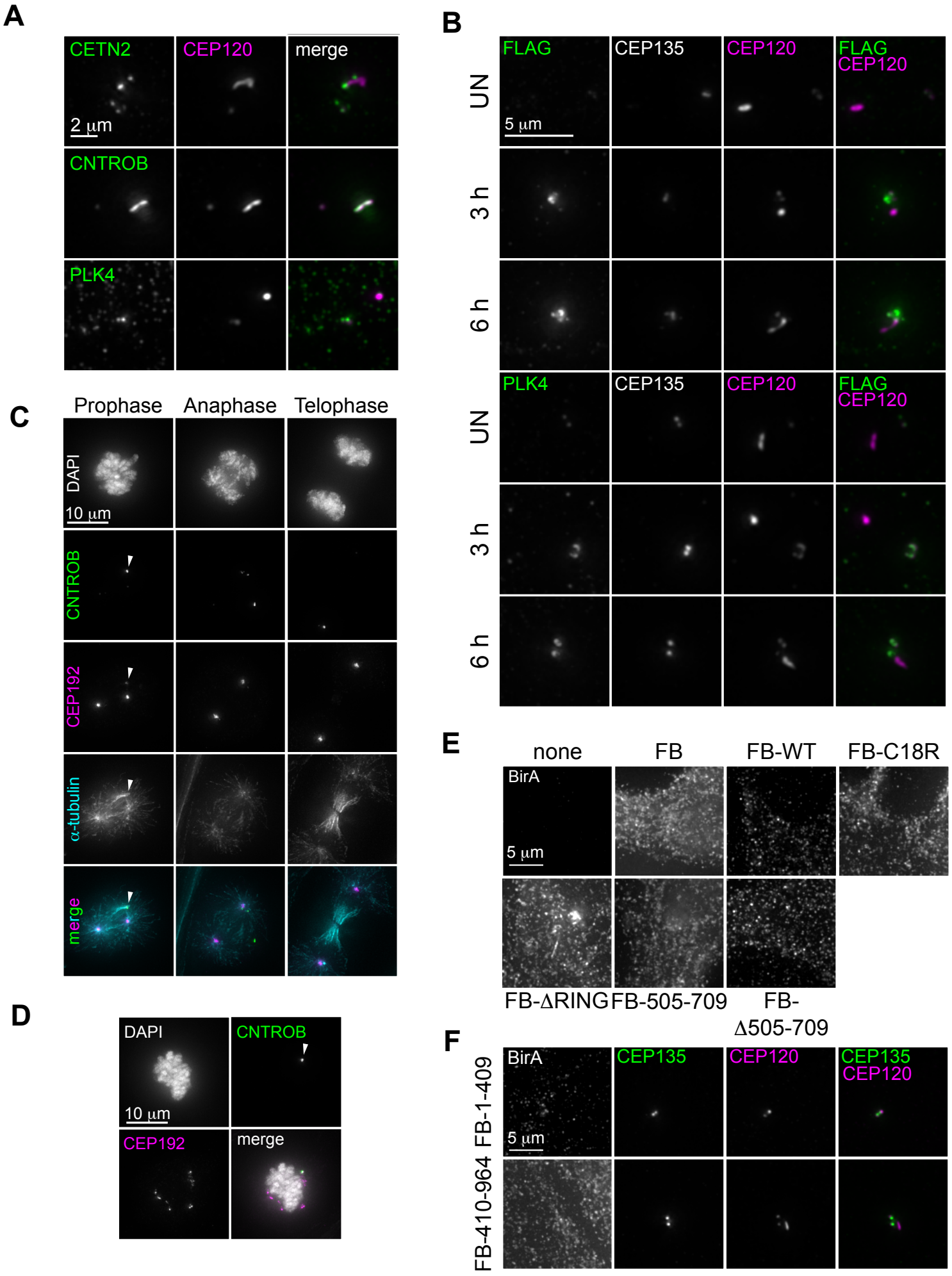

Figure 5 - figure supplement 1

Tkach JM *et al.*

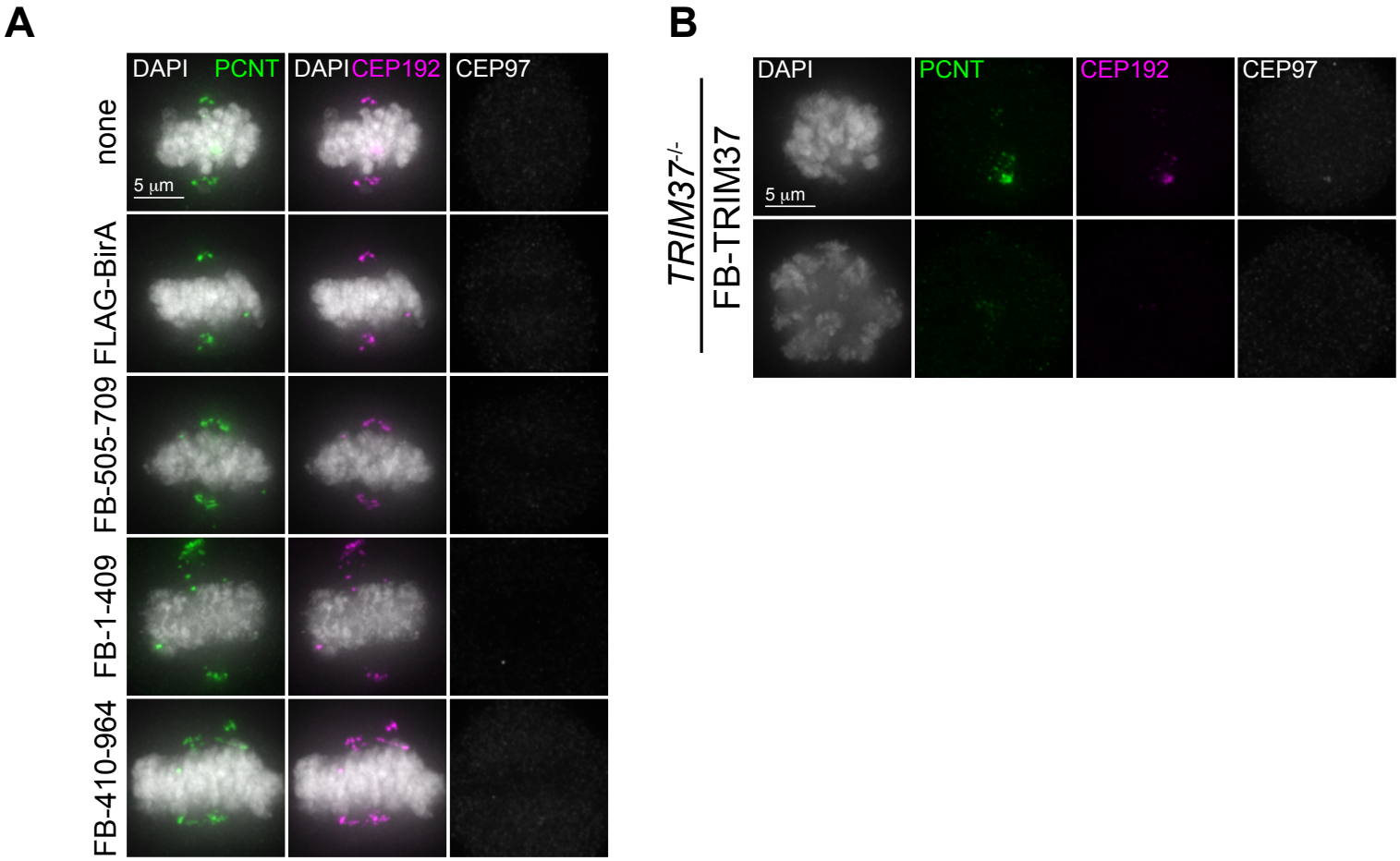

Figure 5 - figure supplement 2

Tkach JM *et al.*

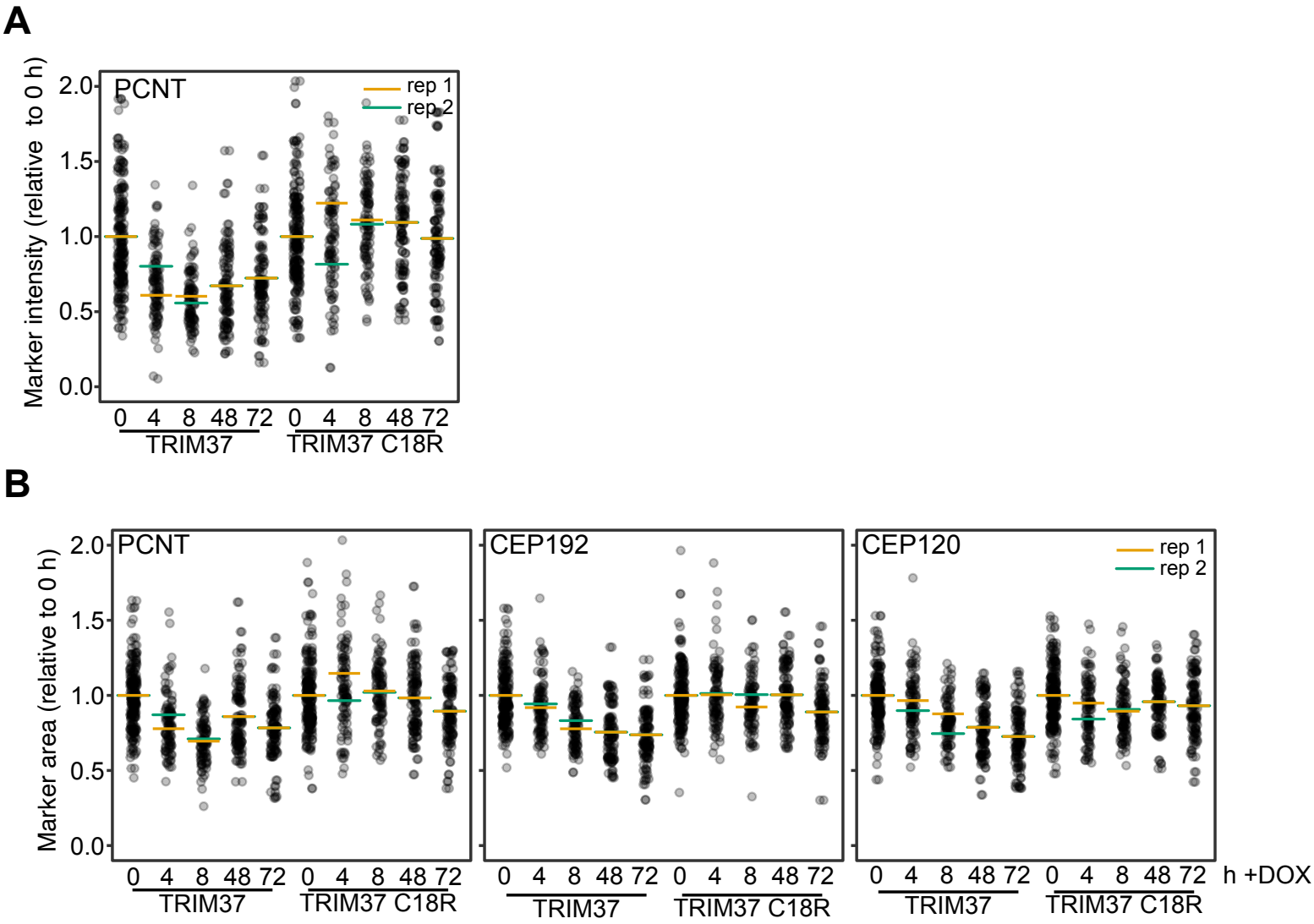

Figure 6 - figure supplement 1

Tkach JM *et al.*